POLITECNICO DI TORINO

Department of Mechanical and Aerospace Engineering
Class LM-33 (DM270)

Master's Degree in Automotive Engineering

Design and validation of an adaptive tyre model with influence of temperature for a Formula SAE Vehicle

Tutors

Prof. Andrea TONOLI

Eng. Stefano FAVELLI

Eng. Raffaele MANCA

Eng. Eugenio TRAMACERE

Candidate

Giovanni Bartolomeo CASSINI

Academic Year 2023/2024

Table of Contents

Abstract

Tyres are essential components of a race car, being the only direct link between the vehicle and the road. In racing environments, it is crucial to model them with a high accuracy level to maximize the performance of the whole vehicle. Common tyre models, such as Magic Formula, are described by a pure mechanical behaviour, neglecting the influence of parameters such as temperature, which has a big effect on force production capability of tyres. Because of that this master thesis proposes an adaptive thermal tyre model, aimed to improve the estimation of tyre forces produced in the contact patch. First, a tyre surface temperature estimator is proposed, which allows to measure this parameter without sensors and a low computational cost. Starting from works already present in literature, a new lumped parameter model with more features is developed. Tyre thermal parameters are defined and fitted using measured data and its performance is evaluated. Then, a modified version of Pacejka's Magic Formula with influence of temperature is proposed, adding new empirical coefficients dependent by temperature. These coefficients are fitted using an updated procedure already used to estimate Magic Formula coefficients. Modified Magic Formula's performance is compared with the base one confirming that the addition of temperature effects results in an better accuracy of tyre forces estimation. Finally, an application of the tyre model is discussed, explaining its role in vehicle control systems.

Chapter 1

Introduction

1.1 Formula Student

Formula Student is an engineering competition in which more than 200 University teams from more than 60 countries are involved. The competition is subdivided into three main categories: Combustion Vehicles, Electric Vehicles and Driverless Vehicles. Squadra Corse PoliTo competes in Electric Vehicle class, which has become the most diffused and competitive in the recent years. As mentioned above, the competition is an engineering challenge, not a racing championship: this means that to succeed in Formula Student events, the team must be excellent in all engineering disciplines. In fact, a typical Formula Student competition is subdivided into Static Events and Dynamic Events. Static Events are three: Engineering Design, Business Plan Presentation and Cost and Manufacturing.
Engineering Design consists of presenting all the engineering choices made by the team during the design phase of the season to obtain the manufactured vehicle. Each choice must be clearly explained and justified to a group of expert judges coming from different automotive companies and belonging to different engineering areas.
Business Plan Presentation consists to simulate a real business plan case study. The target is to find the best innovative business idea to sell the car or everything related to it. An entire financial analysis is needed, from the idea, to the product one, passing from market forecast, marketing and future trends. Everything has to be presented to a team of judges that will act as potential business investors and will decide whether the idea is innovative and the business study has been well conducted.
Finally, Cost and Manufacturing has the target of explaining and justifying the team's costs of the current season, with a focus on the environmental impact of the production of a particular vehicle subsystem.

The dynamic events, instead, directly involve the competing vehicles, even if in the official regulation is clearly stated that any wheel to wheel racing is prohibited. In fact, any point scored by the team in each Dynamic Event is only depending on the relative time difference between the team and the best team on that event (or, concerning the Efficiency event, the relative difference between the consumed energy compared to the best team). The Dynamic events are four: Acceleration, Skidpad, Autocross and Endurance.
Acceleration Event consists of an acceleration from standing still of 75 meters long track, three meters wide. Skidpad event consists of an eight-shaped track with a width of three meters. The two circles drawing the eight shape have a central radius of 9.125 meters. The driver must complete the two right circles and then the two left circles. Only the second run for each side is timed and the final lap-time is the average of the two runs.
Autocross Event is a single lap starting from standing still. The track can be open or closed circuit, generally with a total length of approximately one kilometer, with a minimum track width of three meters. There are other characteristics such as the maximum straights length or minimum hairpins radius.
Finally, Endurance Event, the most important one, consists of a long run race of 22 kilometers, divided into two stints of 11 kilometers each. A driver change is mandatory at the end of the first stint. In this event, vehicle performances are not the key for the victory: tyre and energy management, as well as vehicle overall reliability are the most important factors to succeed.

1.2 Squadra Corse PoliTo

Squadra Corse PoliTO is the Formula Student team of the Politecnico di Torino. Born in 2004 with the target of competing in the Formula student championship, the first vehicle was ready in 2005, racing that summer in the Combustion category.

Figure 1.1: SC05, 2005 prototype

The Internal Combustion Engine prototype development proceeded until 2009, when the first hybrid prototype was designed starting from 2008 prototype. It raced during summer 2010 events, winning the world championship.
The first Electric prototype arrived in 2012, when Squadra Corse PoliTo became

Figure 1.2: SC08H, 2010 prototype

the first Italian team to participate to Formula Stu dent Electric category. From that year up to now, the vehicle has always remained fully electric, pushing the research and development with the target of reducing weight, improving aerodynamic efficiency and improving control strategies. In 2019, SC19 prototype achieved the 1st place overall at Formula ATA, italian Formula SAE event held at Varano de' Melegari.

In the 2024 season the team participated to three events: FSA (Formula Student

Figure 1.3: SC19, 2019 prototype

Austria), FSG (Formula Student Germany) and FSATA (Formula SAE Italy). The team took part to the dynamic events in Germany after eleven years achieving a top 20 position in Acceleration and Skidpad events, while in Italy was capable to end the entire competition without reliability issues obtaining good results.
The team is composed by 70 students coming from 10 different engineering courses, it is organized in different departments, working together to achieve a common goal:

- Aerodynamics & CFD: they are responsible of designing, manufacturing and validating in the wind tunnel all the aerodynamic package of the vehicle. Moreover they perform all CFD analysis of other divisions

- Battery Pack: they are responsible of designing and assembling the low voltage and high voltage batteries of the vehicle.

- Chassis & Composites: they are responsible of designing and manufacturing the vehicle chassis and the impact attenuator. Moreover they are responsible of all studies on composite materials of the vehicle.

- Communication & Media: they are responsible of every social media, content creation and event of the team.

- Electronics: they are responsible of designing and manufacturing all the electronic components present on on-board.

- Management: they are responsible of managing the cash flow of the team, as well as making strong relationships with su ppliers and managing all the Static Events.
- Powertrain: they are responsible of managing, testing and calibrating inverters and motors.
- Thermal Management: they are responsible of designing and manufacturing all the cooling system of the vehicle (battery, inverters, motors).
- Unsprung Masses & Geartrain: they are responsible of designing and manufacturing all the unsprung masses of the vehicle (rim, suspensions, transmission, uprights, braking system) and the steering assembly.
- Vehicle Dynamics & Control Systems: they are responsible of the early season target setting, every full vehicle simulation, suspension kinematics, telemetry, data analysis and the complete control system. Moreover, they are responsible of track tests and driver trainings.

1.3 SC24

SC24 is the prototype designed and built by Squadra Corse PoliTo for season 2024.

Figure 1.4: SC24, 2024 prototype

The vehicle chassis is characterized by a CFRP and aluminum honeycomb sandwich

monocoque, aluminum and steel anti anti-rollover tubes and aluminum honeycomb impact attenuator.
Vehicle is equipped with an aerodynamics package made of front wing, rear wing and sidepods. Front wing has three different configurations to vary downforce and balance by changing the flap angle, as shown in table.

Configuration	Cl (full car)	Cd (full car)	Aero Balance	Efficiency
-1°	-4.96	1.52	0.50	3.26
-3°	-4.90	1.52	0.49	3.22
-5°	-4.83	1.50	0.47	3.22

Table 1.1: Aerodynamics performance for different flap angles

Vehicle suspensions are double wishbone with fully adjustable pushrod layout made of CFRP tubes, connected by uniball joints to the monocoque and to the machined aluminum uprights.
The powertrain, as stated before, is fully electric coming from AMK Formula Student racing kit. It includes four IGBT inverters and four SPM - IPM Electric Motors, each one independently controlled by a single inverter. Each motor guarantees a maximum torque of 21 Nm and maximum velocity of 20000 rpm, reaching up to 35 kW of maximum power. The powertrain is so able to develop 140 kW at 600 V DC, but the power is limited by FSG regulations at 80 kW at the DC battery output bus. Motors are in in-wheel, outboard outboard-mounted, transferring power to tires through a double double-stage planetary transmission with a single gear ratio of 14.69:1.
The High Voltage b attery pack is made of two parallels of 132 series of pouch Li Li-Po cells. The battery pack has a nominal capacity of 7.7 kWh at nominal voltage.
The on on-board signals run through four CANs that are managed by the dSpace MicroAutobox II Electric Control Unit, through the Vehicle Control System installed in it.

1.4 Thesis Outline

This thesis is structured as follows:

- Chapter 2 presents the tyre as a component, starting from its composition to its capability to produce grip and forces.

- Chapter 3 presents tyre testing procedure and its role to collect data about tyre behaviour.
- Chapter 4 presents the tyre thermal models, starting from state of art to a proposed temperature estimator, showing its performance.
- Chapter 5 presents the tyre model, describing Pacejka's Magic Formula and a proposed variation of the model with influence of temperature.
- Chapter 6 presents the conclusion of the project, summarizing its key points.

Chapter 2

Tyre Behaviour

2.1 Tyre Structure

Tyres are the only element that connects the vehicle with the road surface. For this reason they are the primary source of forces and moments that provide motion and handling of the vehicle.
A tyre is composed by different parts, as it's possible to see in each one characterized by different materials and properties:

- Tread: is the most external part of the tyre, the only one in direct contact with the road and subjected to wear. It is made by rubber (mixture of synthetic and natural compounds). The compound is responsible of the grip generation, helping the traction of the vehicle.

- Belt: it is located under the tread and it is made by two layers of steel cords in a radial distribution (typical of a car). The belt helps to maintain the tyre shape, providing support to the rubber structure.

- Carcass: it is the most internal layer of the tyre, it is directly in contact with the inner gas. It is made by a rubber compound, mixed with some polyester or nylon.

- Sidewall: it is an external part of the tyre which helps it to maintain its shape. It is primarily made of rubber compounds but it is reinforced by a variety of materials from flexible metals to plastics. In this way it makes sure that the tyre stays mounted on the rim and provides vertical stiffness.

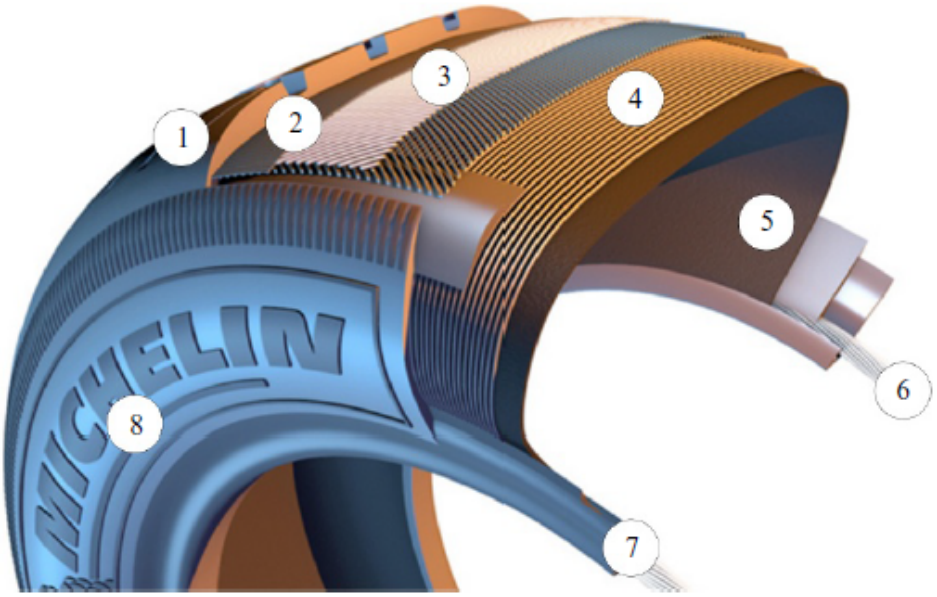

1: Tyre tread
2: Crown belt
3: Crown ply
4: Casing ply
5: Inner liner
6: Bead wire
7: Bead section
8: Sidewall

Figure 2.1: Internal construction of a radial tyre. Reproduced with kind permission of the Michelin Tyre Company (Performance Vehicle Dynamics, 2018)

2.2 Mechanisms of Grip Generation

When the tyre moves on the road friction occurs between the two surfaces that are in contact. The area of the tread in contact with the road is called *contact patch*. This is the place where forces between tyre and road are exchanged thanks to friction and inflation pressure. It changes size and shape when the vehicle is moving and is affected by the following parameters:

- Vertical load: more the tyre is loaded, larger will be the contact patch
- Vehicle speed: faster is the vehicle, smaller is the contact patch
- Tyre pressure: higher pressure implies smaller contact patch
- Tread width: a higher wear decreases the contact patch

Mechanical friction is produced in the contact patch, and a higher friction (grip) allows to transmit higher forces. Therefore, it's fundamental to understand how

grip is generated from a physical point of view.
Two main grip mechanisms are defined:

- Mechanical grip (deformation): a road profile is not flat but it is affected by a certain level roughness. When tyre tread is in contact with the asperities of the road surface, it gets deformed by the road profile. Being tyre rubber a visco-elastic material, during this deformation action-reaction forces are produced, helping the tyre to stick to the road, producing grip

- Chemical grip (adhesion): it is generated by the chemical reaction between tyre compound and track surface aggregate. When the tyre is rolling and comes in contact with the road surface, chemical reactions are produced building momentary molecular bonds (Van der Waals forces). These bonds have an adhesive effect producing grip between the two surfaces.

2.3 Factors Affecting Grip Generation

The two grip mechanisms mentioned above are affected by many factors: tyre temperature, pressure, ambient conditions, tyre carcass design. A particular focus has to be given to the first two, since they are states that characterize the tyre.

2.3.1 Temperature

Tyre behaviour can have a big difference depending on the temperature on which the tyres are run. Tyre temperature affects both the force-producing capability of the tyre and also the life of the tyre. A change in temperature will change the modulus of elasticity of the rubber (unlike belts, made with steel, where this is constant over a large temperature range) and affect the cornering stiffness and grip.

If too cold, tyres are very slippery. An increase in temperature will make the rubber softer allowing it to deform more easily, increasing mechanical grip. In addition, a warmer tyre will be more easily be penetrated by the aggregate, so the chemical reactions governing the bonding will happen more quickly increasing chemical grip. However, increasing the temperature will also reduce material properties, and in particular, the shear modulus and yield stress in shear, reducing performance [**1**]. For this reason, each tyre has a temperature window for correct operation. In a racing tyre around 10 degrees can cause a drop in grip of around 10% (see Figure 2.2), and a cold tyre may have as little as half the grip of one at running temperature.

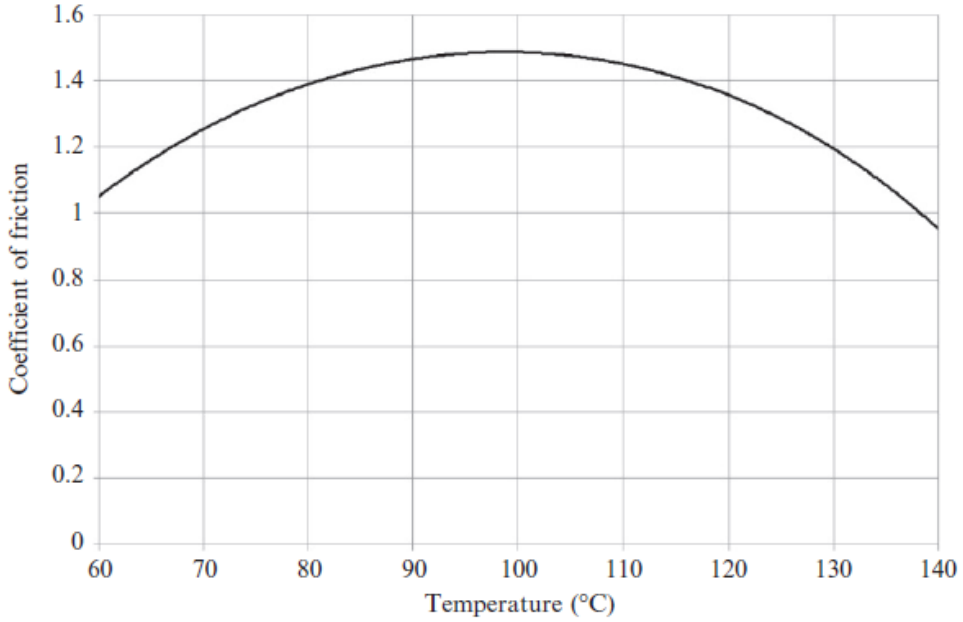

Figure 2.2: Effect of temperature on grip (Performance Vehicle Dynamics, 2018)

2.3.2 Pressure

If a tyre is underinflated or overinflated, its performance will be compromised. In fact, if the tyre is not correctly inflated, the carcass will be out of shape, and the contact patch area reduced. Overinflation makes the tyre running only on the centre of the contact patch. As a consequence, the central region gets overheated since a level of shear force sufficient for the whole tyre passes though a reduced region. This reduces the level of grip beyond that loss expected from the ratio of areas involved. While in a underinflated tyre most of the load is carried on the outer regions of the contact patch and similar problems are encountered.

2.4 Tyre Forces and Moments

A tyre can be represented as a body with six degrees of freedom that operates between the road surface and the wheel's stub axle. Since tyres are elastic, the forces they produce are related to the deflection they have in each degree of freedom. In this way it's possible to define the following forces and moments for each tyre: Fx, Fy, Fz, Mx, My, Mz. A brief description of longitudinal and lateral forces is given since they make the most relevant contribution to vehicle motion and handling.

2.4.1 Longitudinal Force

In order to understand how a longitudinal force is produced by the tyre it's important to mention what is the rolling radius. When a rigid wheel is in "free rolling" condition, without any braking or traction moment applied, its rolling radius R is simply defined by the relationship between the forward speed V and the angular velocity ω

$$V = \omega R \tag{2.1}$$

While loaded radius R_l is defined as the distance between the wheel axis and the ground. However in a pneumatic tyre the tread band is compliant resulting in a centre of instantaneous rotation not coincident with the contact centre. The distance between the wheel axis and the centre of instantaneous rotation is called effective rolling radius R_e and is computed as

$$V = \omega R_e \tag{2.2}$$

Typically in free rolling it results that $R_l < R_e < R$.

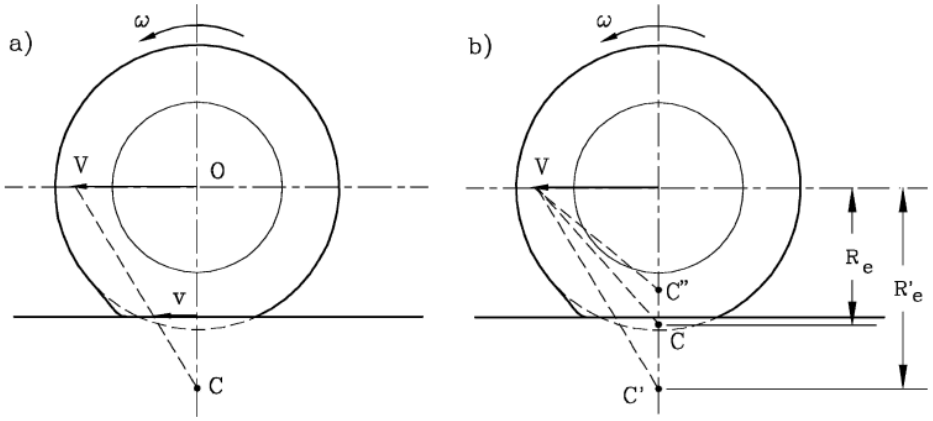

Figure 2.3: (a) Braking wheel, center of instantaneous rotation and slip speed. (b) Position of the instantaneous rotation center by pure rotation C, by braking C' and by traction C" (The Automotive Chassis - Vol. 1, 2009)

Consider a pneumatic wheel rolling on level road on which a braking moment is applied. As it's described by Giancarlo Genta in [**2**], the tread band is circumferentially stretched in the zone that precedes the contact with the ground, The

effective rolling radius, whose value in free rolling was between R_l and R, grows towards R and, if if the braking moment is large enough, becomes greater than R. Therefore, with the help of Figure 2.3, it's possible to say that

$$\omega R_e < V \tag{2.3}$$

In this way it's possible to define a longitudinal slip σ as

$$\sigma = \frac{\omega Re}{V} - 1 \qquad -1 \leq \sigma \leq 0 \tag{2.4}$$

While if a traction moment is applied, the leading part of the contact zone is compressed and not stretched. For this reason,

$$\omega R_e > V \tag{2.5}$$

and slip is computed as

$$\sigma = 1 - \frac{\omega Re}{V} \qquad 0 \leq \sigma \leq 1 \tag{2.6}$$

Where the longitudinal slip velocity v_s is defined as

$$v_{sx} = V - \omega Re \tag{2.7}$$

However, there is not an actual sliding of the contact zone as a whole. Actually the peripheral velocity of the leading part is still , and it's called non-sliding area. The sliding area, or slip zone, begins only at the point indicated in Figure 2.4.

Increasing the slip the sliding area becomes larger up to reaching the leading part of the contact zone, as depicted in Figure 2.4. When this condition is reached, global sliding of the tyre occurs.
The longitudinal Force F_x that the wheel exchanges with the road is a function of the slip

$$F_x = C_\sigma \sigma \tag{2.8}$$

It is null at $\sigma = 0$ and increases linearly for small values of σ, usually between -0.25 and 0.25. C_σ is defined as slip stiffness of the tyre. Outside the linear range, sigma decreases up to -1 (locking wheel), while in driving conditions it can increase up to infinite (slipping tyre). F_x-σ characteristics depends by many factor, in particular

by vertical load. Increasing F_z the slope of the linear range increases too along with its peak.

Normalized longitudinal force, or longitudinal friction coefficient, can be computed as:

$$\mu_x = \frac{F_x}{F_z} \tag{2.9}$$

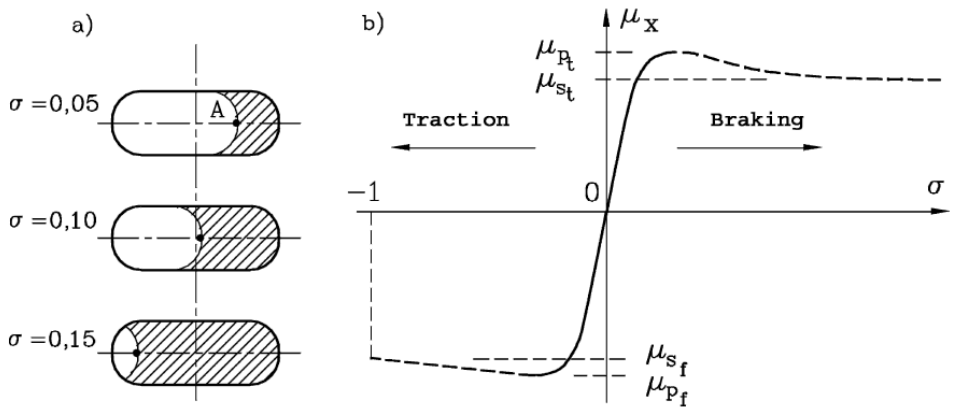

Figure 2.4: (a) Slipping area at different values of slip σ. (b) Qualitative diagram of μ_x as function of longitudinal slip σ.

Longitudinal friction coefficient has a dependency from the longitudinal slip, resulting in a linear range for small values up to a certain peak, then decreasing for higher values. Road conditions can affect the peak friction coefficient, e.g. if there is a wet road μ_x has a much lower peak, resulting in a poor grip surface. Worse results can be obtained from snow or icy roads (Figure 2.5).

2.4.2 Lateral Force

In the previous section it became clear that a longitudinal force can occur only if slip is present, therefore if deformations are present in the tread band. The generation of lateral forces in the road-wheel contact is dependent too by the compliance of the tyre. As it's explained in [**2**], if the wheel centre velocity doesn't lie in its mean plane, the shape of the contact zone is distorted.

Consider a point on the mean plane on the tread band (Figure 2.6), upon approaching the contact zone it tends to move in a direction parallel to the velocity V, relative to the centre of the wheel, and consequently goes out of the mean plane. After touching the ground at point A, it continues following the direction of the velocity V until it reaches point B. At that point, the elastic forces pulling it

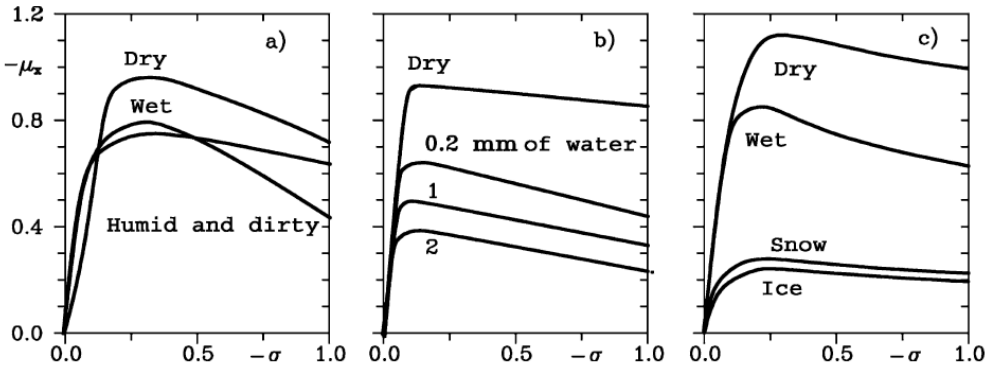

Figure 2.5: Curves of $\mu_x(\sigma)$ obtained in different conditions (The Automotive Chassis - Vol. 1, 2009)

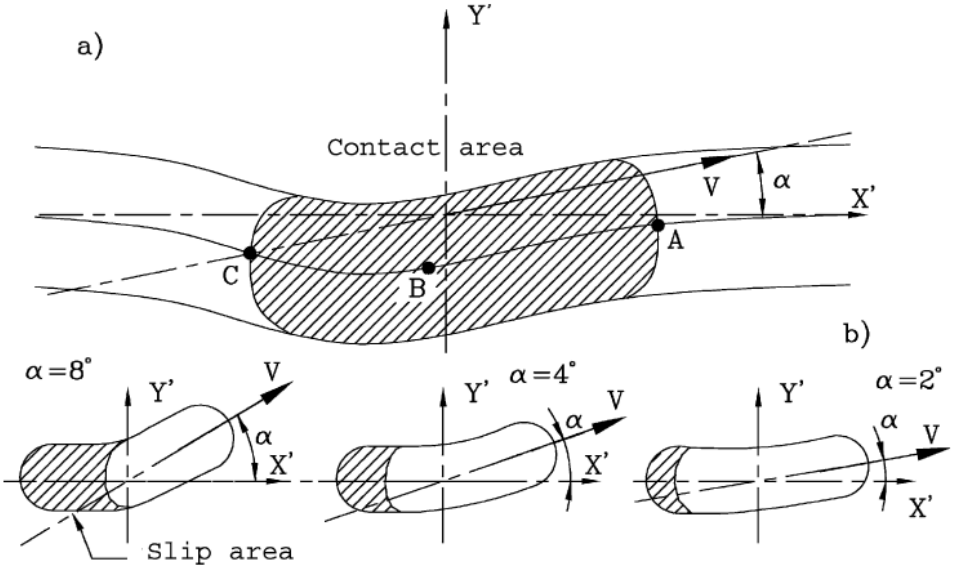

Figure 2.6: Wheel-road contact when side slip angles are present. (a) Contact zone and path of a point of the tread on the equator plane; (b) contact zone and slip zone at different values of side slip angle (The Automotive Chassis - Vol. 1, 2009)

towards the mean plane are strong enough to overcome those due to the friction on the road, forcing it to slide on the road and to deviate from its path. This sliding continues for the remaining part of the contact zone until point C is reached. The contact zone can be divided into two parts: a leading zone in which no sliding occurs and a trailing zone in which the tread slips towards the mean plane. This

second zone grows with the side slip angle, until it pervades the entire contact zone and the wheel actually slips on the ground. The angle between the direction of velocity vector and the mean plane of the wheel is called side slip angle α and is defined as:

$$\tan \alpha = \frac{V_y}{V_x} \tag{2.10}$$

As in the longitudinal case, the lateral force is plotted as function of the slip angle, it grows linearly with increasing alpha up to a certain value

$$F_y = -C\alpha \tag{2.11}$$

Where C is called cornering stiffness, after the linear range lateral force remains constant or decreases slightly because sliding condition is reached.

Also in this case it's possible to define the normalizes lateral force, or lateral friction coefficient as

$$\mu_y = \frac{F_y}{F_z} \tag{2.12}$$

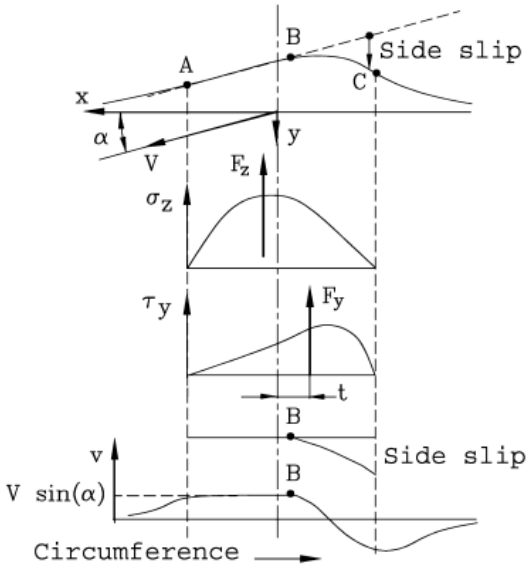

Figure 2.7: Lateral deformation, distribution of pressures, slip and lateral speed in a cornering tire (The Automotive Chassis - Vol. 1, 2009)

The lateral deformations of the tire are showed in a qualitative way in Figure 2.7. It's possible to see that the resultant F_y of the distribution of side forces is

not applied at the centre of the contact patch but at a point that is located behind it with a distance t. This distance is defined as pneumatic trail, that produces the aligning moment

$$M_z = F_y t \tag{2.13}$$

as it tends to force the mean plane of the wheel towards the direction of the velocity V. Both lateral force and aligning moment depend on many factors such as vertical load, pressure, road conditions etc.
Lateral behaviour of the tyre can be described in a single diagram, the Gough diagram, in which the lateral force is plotted against the self-aligning moment, as in Figure 2.8.

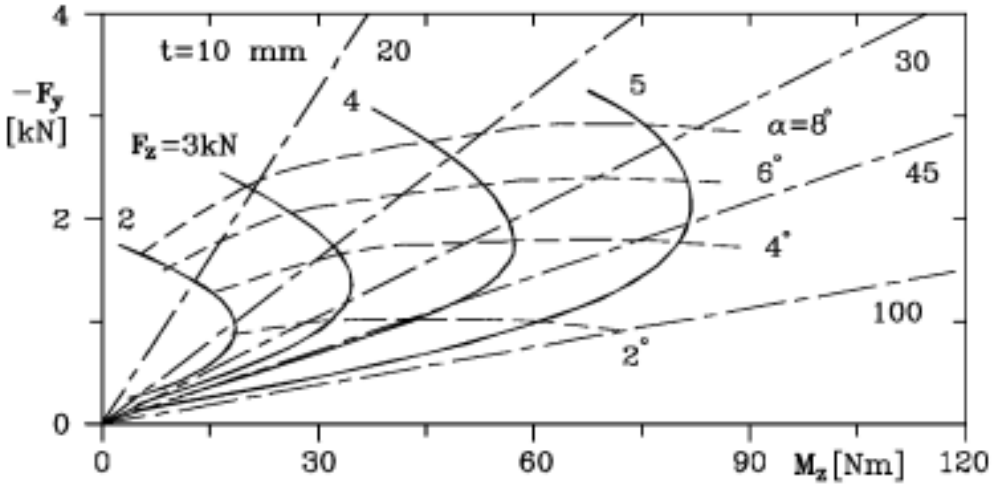

Figure 2.8: Example of Gough diagram (The Automotive Chassis - Vol. 1, 2009)

Lateral force can be produced also with null side slip angle, if a camber angle is present. Camber angle can be defined as the inclination of the vertical mean plane of the tyre with respect to the y axis. It is usually called camber thrust or camber force, as distinct from cornering force, which is due to side slip angle alone. The camber force added to the cornering force gives the total side or lateral force, but the camber force is usually far smaller than the cornering force.

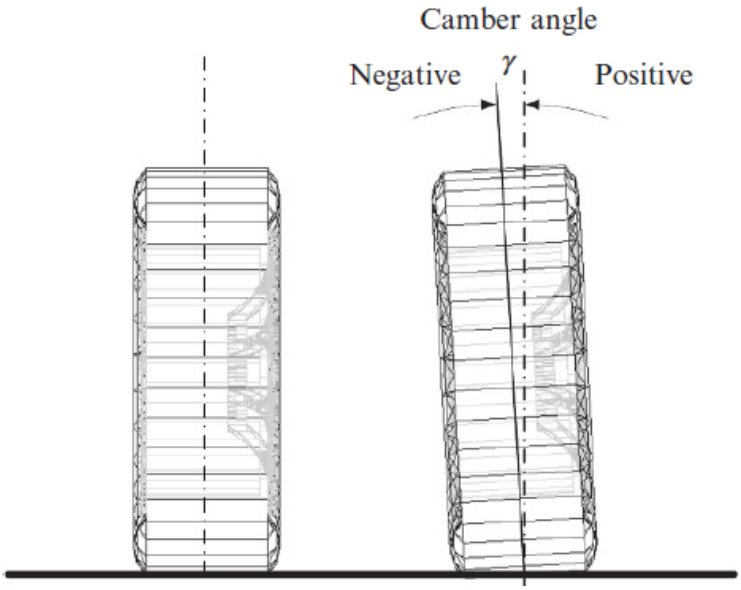

Figure 2.9: Representation of camber angle (Performance Vehicle Dynamics, 2018)

Chapter 3

Tyre Testing

3.1 Overview

Since simulation can only provide an approximation and many tyre models rely on empirically determined parameters, tyre testing is required to measure its characteristics. Tyre testing can be done indoor or outdoor:

- Indoor testing: indoor tests in laboratory are typically done using a belt or a drum machine. Tyre is made rolling along a steel belt and held in position with an adjustable and rigid support structure. The main advantage is that the test is conducted in a controlled environment. Camber, slip angle, speed, load, pressure and temperature can all be monitored and varied under control. On the other hand, the steel belt is not a real road material, therefore a corrector coefficient (scaling factor) is needed to adapt the obtained results to real road ones.

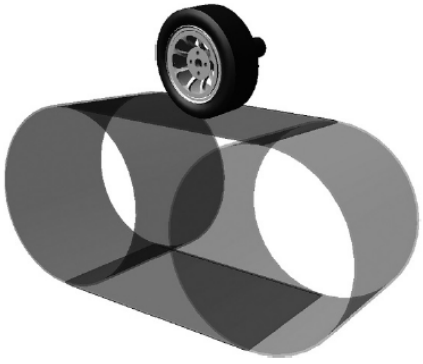

Figure 3.1: Belt tyre testing machine (Performance Vehicle Dynamics, 2018)

- Outdoor testing: tyres can be tested outdoor using a trailer. The test tyre is mounted underneath the trailer and kept in contact with the road surface. The trailer itself must be sufficiently large and heavy that the lateral and longitudinal forces developed by the tyre under test are negligible compared with those generated by trailer's tyres. Also in this case it's possible to control all tyre parameters.
  Another approach is to use a wheel force transducer (WFT), which is a sensor mounted directly between rim and stub axle. Through this method it's possible to measure with high accuracy the loads in all six degrees of freedom on a real road surface. However, it is a very sophisticated and expensive system.

Figure 3.2: Wheel force transducer (https://tyrecaenotebook.wordpress.com)

3.2 FSAE Tire Test Consortium

FSAE Tire Test Consortium (FSAE TTC) [**3**] is an organization that conducts periodically tyre force and moment tests and makes the data available for Formula Student teams. Tests are performed at Calspan Tire Research Facility (US), which provides a flat belt testing machine. All the tyres tested by Tire Test Consortium perform cornering and drive-brake tests, in which variables such as load, slip angle, slip ratio, inclination angle and pressure are swept. From each test the following data channels are collected:

These data are fundamental for tyre companies or whoever does research and development on tyres to characterize their models. As it is explained with more accuracy in the next chapters, tyre models are empirical and contain coefficients

Channel	Units	Description
AMBTMP	degC or degF	Ambient room temperature
ET	sec	Elapsed time for the test
FX	N or lb	Longitudinal Force
FY	N or lb	Lateral Force
FZ	N or lb	Normal Load
IA	deg	Inclination Angle
MX	N-m or lb-ft	Overturning Moment
MZ	N-m or lb-ft	Aligning Torque
N	rpm	Wheel rotational speed
NFX	unitless	Normalized longitudinal force (FX/FZ)
NFY	unitless	Normalized lateral force (FY/FZ)
P	kPa or psi	Tire pressure
RE	cm or in	Effective Radius
RL	cm or in	Loaded Radius
RST	degC or degF	Road surface temperature
SA	deg	Slip Angle
SL	unitless	Slip Ratio based on RE (such that SL=0 gives FX=0). This is "traditional" or "textbook" slip ratio.
SR	unitless	Slip Ratio based on RL (used for Calspan machine control, SR=0 does not give FX=0). Hint: use SL instead of SR.
TSTC	degC or degF	Tire Surface Temperature--Center
TSTI	degC or degF	Tire Surface Temperature--Inboard
TSTO	degC or degF	Tire Surface Temperature--Outboard
V	kph or mph	Road Speed

Figure 3.3: Tire Test Consortium data channels

which have to be determined. For this reason tyre test data become essential to estimate them and make the model representing tyre behaviour with the highest possible accuracy.
As it is explained more in Chapter 5, tyre model has inputs and outputs, data channels include both of them. In Figure 3.4 an example of inputs variable is shown, such as vertical load, inclination angle, pressure. It's very important to know that input values are not random but have a specific trend. In fact, during a flat trac test session specific conditions at which the tyre is run are defined. In this case it's clear to see that the vertical load is measured at 5 different ranges (the blue spots in the 1st subplot), while inclination angle and pressure at 3 different ranges. These ranges are fundamental for the fitting procedure that is described in Chapter 5.

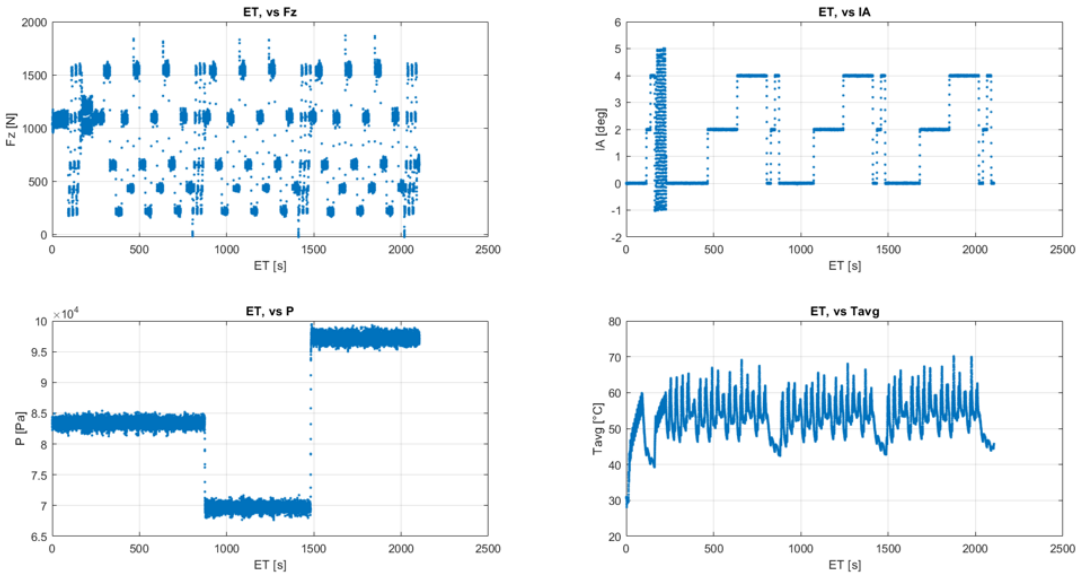

Figure 3.4: Example of inputs variables from a flat trac test (Tire Test Consortium)

Chapter 4

Tyre Thermal Models

4.1 State of art

It is demonstrated that temperature affects tyre behaviour influencing its force production capability. These changes include the temperature dependency of friction coefficients and the loss of cornering stiffness with increasing temperature. To account these effects and improve accuracy of tyre forces, it becomes essential to reliably estimate tyre temperatures using information gathered from sensors or state estimators the vehicle can provide. This needs to be done in real time and therefore a reasonable compromise between accuracy and computational time has to be achieved.

This chapter describes the current state of art of various thermal models that are applied to existing tyre models. Then, a new temperature estimator is proposed, based on an improvement of current models available in literature, with a focus on the estimation of its thermal parameters and an analysis of its performance with respect to the temperature obtained from measurements.
The models used for benchmark analysis are those from Aldo Sorniotti and the one developed by A. J. Tremlett & D. J. N. Limebeer, due to their simplicity and relatively accurate output results.

4.1.1 1DOF Model

This model, proposed by Prof. Aldo Sorniotti [**4**], represents the tyre as an equivalent thermal capacity C_{eq}, which is subjected to different power fluxes that are described below. The structure of the model is shown in Figure 4.1.

- A power flux ($P_{rolling\_resistance}$) related to tyre rolling resistance, resulting in internal dissipation to the carcass.

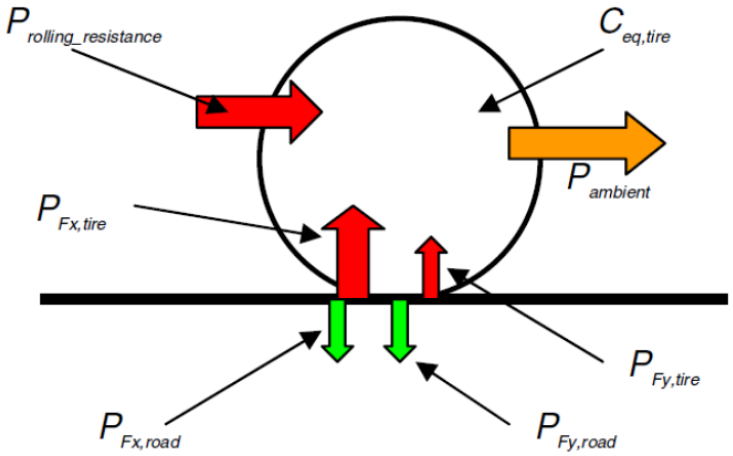

Figure 4.1: 1DOF model schematic

- A power flux related to the generation of longitudinal force because of longitudinal slip. A fraction λ of this energy is dissipated at the contact patch and enters the tyre ($P_{Fx,tyre}$) while the remaining part heats the road surface ($P_{Fx,road}$).
- A power flux related to the generation of lateral force because of lateral slip. A fraction λ of this energy is dissipated at the contact patch and enters the tyre ($P_{Fy,tyre}$) while the remaining part heats the road surface ($P_{Fy,road}$).
- A power flux ($P_{ambient}$) related to the cooling flux produced by the temperature difference between tyre tread and ambient air.

The state equation of the model is obtained applying the first principle of thermodynamics and considering the power fluxes mentioned above:

$$C_{eq,tyre}\frac{dT}{dt} = P_{rolling\_resistance} + P_{Fx,tyre} + P_{Fy,tyre} + P_{ambient} \tag{4.1}$$

where,

$$P_{Fx\_tyre} = \lambda|(F_x v_{sx})| \tag{4.2}$$

$$P_{Fy\_tyre} = \lambda|(F_y v_{sy})| \tag{4.3}$$

$$P_{ambient} = h(T_{ambient} - T) \tag{4.4}$$

$$P_{rolling\_resistance} = k_r|(F_z v_x)| \tag{4.5}$$

Where h is the thermal exchange coefficient between tyre and ambient, and k_r is the rolling resistance coefficient.
The state equation is a first order differential equation from which the tyre temperature can be computed.
The main drawback of this model is that the equivalent capacity $C_{eq,tyre}$ doesn't account for the different tyre layers composition, resulting in a less accurate estimation of tyre tread temperature.

4.1.2 2DOF Model

The 2DOF model, developed too by Aldo Sorniotti [**4**], divides the tyre in an external layer, representing tread surface, and an internal one, representing the internal carcass. In this way two thermal capacities $C_{eq,tread}$ and $C_{eq,carcass}$ are defined, taking into account the different temperature dynamics of the carcass (lower frequency) and the tread of the component (higher frequency dynamics). The structure of the model is shown in figure 4.2.

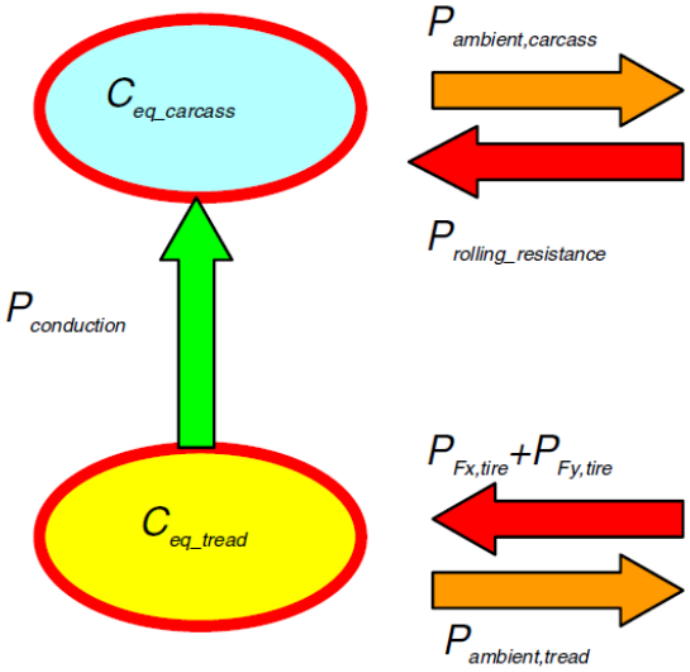

Figure 4.2: 2DOF model schematic

The tread is subjected to the power fluxes related to friction forces and heat transfer between tread and ambient air, while the carcass is subjected to the power fluxes related to rolling resistance and heat exchange with ambient air. A further heat flux is added (P_{cond}) that takes into account the heat exchange between tread and carcass.
The state equations of the model are the following:

$$C_{eq,tread}\frac{dT_{tread}}{dt} = P_{Fx,tyre} + P_{Fy,tyre} - P_{cond} + P_{ambient,tread} \tag{4.6}$$

$$C_{eq,carcass}\frac{dT_{carcass}}{dt} = P_{rolling\_resistance} + P_{cond} + P_{ambient,carcass} \tag{4.7}$$

where,

$$P_{ambient,tread} = h_{tread}(T_{ambient} - T_{tread}) \tag{4.8}$$

$$P_{ambient,carcass} = h_{carcass}(T_{ambient} - T_{carcass}) \tag{4.9}$$

$$P_{cond} = h_{cond}(T_{tread} - T_{carcass}) \tag{4.10}$$

The higher number of states captures more dynamics related to internal and external heat transfers and thus produces better results. However, the main drawback of this model is that it doesn't consider the conduction heat exchange between tyre tread and road surface.

4.1.3 1DOF Model with Tread-Road Conduction

In this model, proposed by A. J. Tremlett & D. J. N. Limebeer [**5**], thermal behaviour of tyre surface temperature is represented using a more detailed 1DOF lumped parameter model that describes the heat fluxes through the isotropic thermal tyre mass.
The main heat flows considered are shown in Figure 4.3 and consist of:

- Q_1: heat generation in the sliding region of the contact patch
- Q_2: heat generation due to tyre carcass deflection
- Q_3: convective cooling through ambient air surrounding tyre
- Q_4: conductive cooling in the non-sliding region of the contact patch

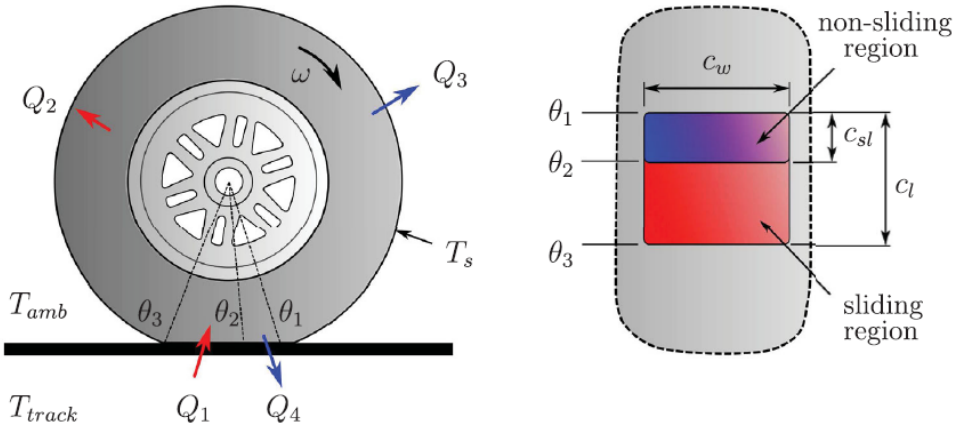

Figure 4.3: 1DOF model with tread-road conduction schematic

Tyre contact patch is divided in non-sliding and sliding region, as described in [**6**]. Angle θ_1 defines the angle at which ground contact is first made with the non-sliding region. Angle θ_2 defines the start of the sliding region, whilst θ_3 marks the end of ground contact.

Tyre tread surface (T_s) is described by the following equation:

$$m_t c_t \frac{dT_s(t)}{dt} = Q_1 + Q_2 - Q_3 - Q_4 \tag{4.11}$$

where c_t is the specific heat capacity of tyre tread and m_t its mass.

Friction power Q_1 generated in the sliding region is computed similarly as in 4.1.1:

$$Q_1 = p_1 u_n (|F_x \kappa| + |F_y tan\alpha|) \tag{4.12}$$

Heat generation due to tyre deflection is represented as a result of longitudinal, lateral and normal tyre forces:

$$Q_2 = u_n (p_2 |F_x| + p_3 |F_y| + p_4 |F_z|) \tag{4.13}$$

Convective cooling through ambient air is dealt with using Newton law, where the heat transfer coefficient term $p_5 u^{p_6}$ is a nonlinear function of vehicle speed:

$$Q_3 = p_5 u_n^{p_6} (T_s - T_{amb}) \tag{4.14}$$

Conductive cooling through non-sliding region of the contact patch is determined by:

$$Q_4 = h_t A_{cp}(T_s - T_{track}) \tag{4.15}$$

where h_t is the heat transfer coefficient between track and tyre, and A_{cp} the non-sliding area of the contact patch. Contact patch area is determined from the vertical load F_z, more details are discussed in [**5**].

These six parameters p_1 to p_6, as well as the thermal parameters of Sorniotti's models, have to be determined through an optimization problem which has the aim to estimate parameters values in order to match model outputs with real measurements. A deeper discussion of the problem is described in 4.2.2.

4.2 Proposed Temperature Estimator

Benchmark models have been analysed looking their strengths and weaknesses and a custom temperature estimator, called *2DOF EVO*, has been designed trying to join the positive aspects of them.

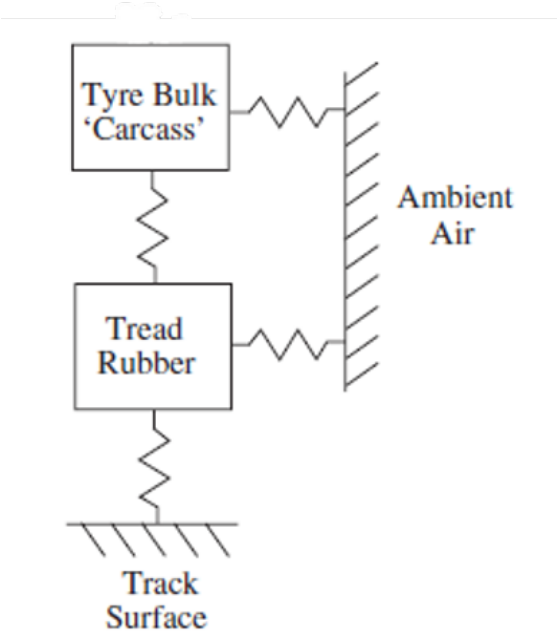

Figure 4.4: 2DOF model schematic

4.2.1 Model Description

2DOF EVO model follows the approach taken in the 2DOF model, since the division in internal and external layer provides a more accurate dynamics of tread temperature. However, from Tremlett and Limebeer's work tread-road conduction and 3-axes tyre deflection effects are added to improve model results.

The state equations of the model are:

$$C_{eq,tread}\frac{dT_{tread}}{dt} = P_{Fx,tyre} + P_{Fy,tyre} - P_{tread,carcass} + P_{ambient,tread} - P_{tread,road} \tag{4.16}$$

$$C_{eq,carcass}\frac{dT_{carcass}}{dt} = P_{deflection} + P_{tread,carcass} - P_{ambient,carcass} \tag{4.17}$$

While the heat exchange relations are:

$$P_{Fx\_tyre} = \lambda|(F_x v_{sx})| \tag{4.18}$$

$$P_{Fy\_tyre} = \lambda|(F_y v_{sy})| \tag{4.19}$$

$$P_{deflection} = v_x(E_x|F_x| + E_y|F_y| + E_z|F_z|) \tag{4.20}$$

$$P_{tread,carcass} = h_{tread,carcass}(T_{tread} - T_{carcass}) \tag{4.21}$$

$$P_{ambient,tread} = h_{tread}(T_{ambient} - T_{tread}) \tag{4.22}$$

$$P_{ambient,carcass} = h_{carcass}(T_{ambient} - T_{carcass}) \tag{4.23}$$

$$P_{tread,road} = H_{tread,road}A_{cp}(T_{tread} - T_{road}) \tag{4.24}$$

Model inputs are:

- Contact patch forces F_x, F_y, F_z $[N]$
- Tyre longitudinal speed v_x $[m/s]$
- Tyre longitudinal slip σ $[-]$ and side slip angle α $[deg]$
- Road surface temperature T_{road} $[°C]$ and ambient air temperature $T_{ambient}$ $[°C]$

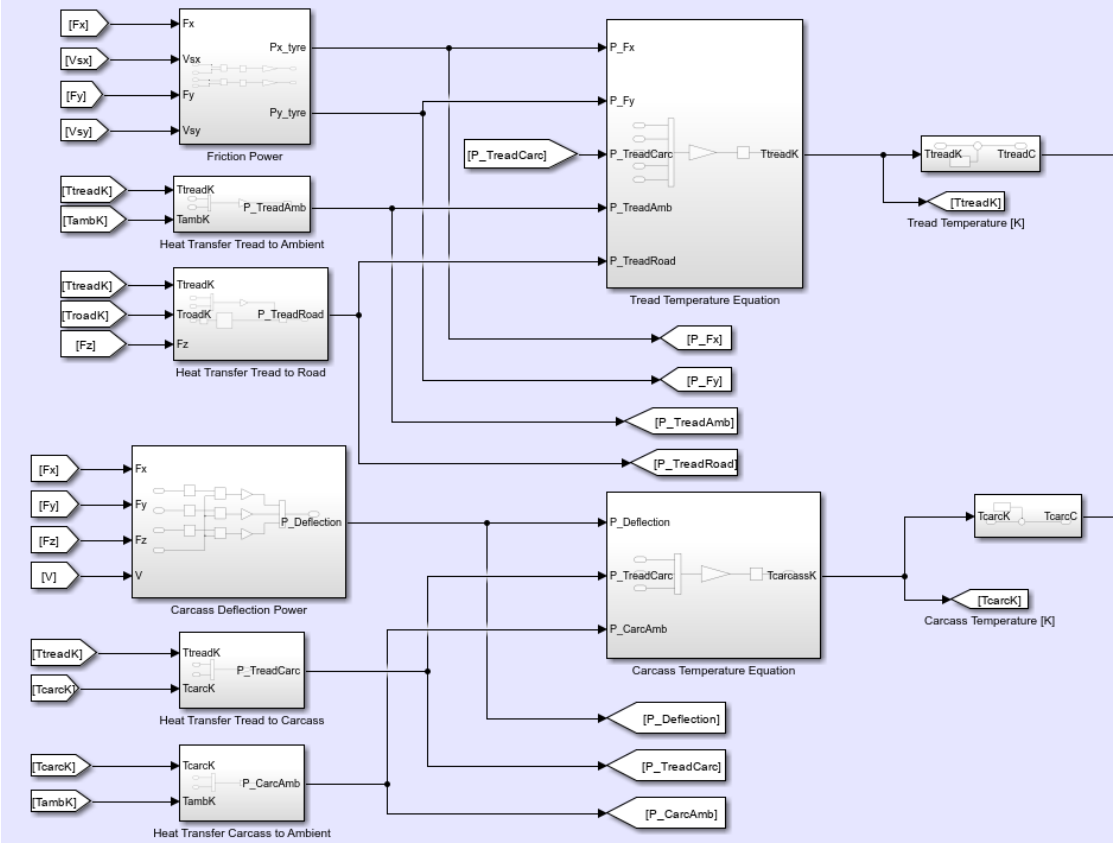

Figure 4.5: Tyre temperature estimator, Simulink scheme

4.2.2 Parameter Estimation

Thermal model equations contain parameters that are unknown. They depend mostly on tyre material properties, which differ among different kind of tyres. Because of that, these parameters, reported in the table below, have to be estimated. FSAE Tire Test Consortium provides test bench data, including all model inputs and tyre tread measurement, which is model output. In this way, through a least squares optimization algorithm that minimizes the error between TTC tread measurement and the one provided by the model, the thermal parameters can be estimated.
In this work the TTC test data from Formula SAE tyre Continental 205/470 R13 are used to calibrate the model, with the aim to obtain the thermal parameters of this tyre. The optimization is carried out using Simulink Design Optimization (SDO) MATLAB add-on. SDO includes a tool called Parameter Estimator that allows to estimate parameters and states of a Simulink model using measured data. The software formulates parameter estimation as an optimization problem, the

Symbol	Description	Units
$C_{eq,tread}$	Tread equivalent thermal capacity	J/K
$C_{eq,carcass}$	Carcass equivalent thermal capacity	J/K
$h_{tread,carcass}$	Heat transfer coefficient tread - carcass	W/K
$h_{tread,ambient}$	Heat transfer coefficient tread - ambient air	W/K
$h_{carcass,ambient}$	Heat transfer coefficient carcass - ambient air	W/K
$H_{tread,road}$	Heat transfer coefficient tread - road surface	W/(m^2K)
λ	Fraction of friction power absorbed by the tyre	-
E_x	Carcass longitudinal force efficiency factor	-
E_y	Carcass lateral force efficiency factor	-
E_z	Carcass vertical force efficiency factor	-

Table 4.1: Temperature Estimator Parameters

optimization problem solutions are the estimated parameter values. In this case, the high availability of data from TTC allowed to use some datasets for estimation and others to validate model parameters. Inside the tool it's possible to choose the optimization method, which is in this case a nonlinear least squares.
In an estimation problem like this one it's crucial to select properly parameter's bounds for two reasons:

1. If no bounds are introduced the optimization may lead to infinite or null values, which are of course unfeasible.

2. Most importantly, many of these parameters (e.g. thermal capacities C_{eq} and thermal exchange coefficients h) have a physical meaning. Their precise value is unknown, since it depends by the tyre specification, however their order of magnitude is, so adding bounds allows to obtain more realistic results.

A deep analysis of works already present in literature has been performed in order to find references about the obtained values of their thermal parameters. Some works, like [**7**], provided accurate numerical values of parameters but using a FEA approach, which is not very suitable with the proposed temperature estimator that is a lumped parameter model. Other works, which are mentioned below, that used a lumped parameter model, make their results suitable for this case. Consider that these works are done on tyres that are different from the one analysed in this thesis, therefore the values would be of course different from the target, however they are very useful to get their order of magnitude, therefore to define

the bounds of the optimization algorithm and allow it to get a better estimation of the parameters.
The references from the following authors have been considered:

- D. P. Kelly & R. S. Sharp [**6**]
- A. J. Tremlett & D. J. N. Limebeer [**5**]
- W. J. West & D. J. N. Limebeer [**8**]
- A. Hackl, C. Scherndl, W. Hirschberg & C. Lex [**9**]

Parameter	Units	[6]	[5]	[8]	[9]
$c_{eq,tread}$	kJ/kgK	1.8	1.8	2.4	1.9
$c_{eq,carcass}$	kJ/kgK	1.8	-	1.6	-
$h_{tread,amb}$	W/K	$2v_x + 10$	$0.018v_x^{1.71}$	(as Ref 2)	6
$h_{carcass,amb}$	W/K	30	-	-	4
$h_{tread,carc}$	W/K	-	-	-	-
$H_{tread,road}$	W/m^2K	12000	12000	12000	1500
λ	no unit	-	0.4	0.6	-
E_i	no unit	0.03	0.01	0.05	-

Table 4.2: Thermal parameters values from references

In Table 4.2 are showed all the values obtained from the analysed references. From these results it's possible to draw several consequences about the thermal parameters:

- $c_{eq,tread}$ and $c_{eq,carcass}$: all the references provide similar values of the specific thermal capacities, giving a good reference concerning the estimation bounds.
- $h_{tread,amb}$ and $h_{carcass,amb}$: heat transfer coefficients with ambient air are about the same order of magnitude because one of the bodies is fixed (air) and the others are similar (tread and carcass). Also, some works ([**6**], [**5**], [**8**]) modelled the tread-air heat exchange considering dependence of speed: if the air speed increases, the tread is surrounded by more air and more cooled. However, in the optimization heat exchange coefficients are all estimated to a fixed value, neglecting the effect of speed. The reason is that TTC data used for validation refer to steady-state tests so it's not possible to estimate these parameters with respect to tyre speed.

- $H_{tread,road}$: three references out of four provide the same value of tread-road conduction, equal to 12000 W/m^2K. However, a study conducted by A. Hackl [**9**] provides a much lower value, equal to 1500 W/m^2K.
  To explain this clear difference it is useful to mention the work made by P. Cattani, L. Cattani and A. Magrini [**10**]. In fact, they underline that one of most adopted values for $H_{tread,road}$ is 12000 W/m^2K and that, in many models and papers, it is used without considering the boundary conditions, such as the tyre rolling speed. For this reason they proposed a speed-dependent empirical equation for $H_{tread,road}$ which confirms that this value is referred to a very high speed (150 km/h), typical of an F1 car, while at a lower speed (e.g. 40 km/h, the one used at TTC tests), $H_{tread,road}$ decreases of more than a half. This behaviour has been seen during the optimization phase too: in a first moment, where higher bounds were introduced (based on high speed value), the algorithm lead to very poor results, while when they have been decreased to a lower value the optimization provided much better results.
- λ and E_i: all the works provide similar values concerning the friction power and the deflection one, giving a solid reference for the optimization bounds.

4.2.3 Results

The analysis made above about the parameters used in literature helps to define the bounds for the optimization algorithm. Upper/lower bounds are reported below with the initial value (the average value of the bounds) because it was noted during the simulations that had an influence on the final results.

Parameter	Units	Lower bound	Upper bound	Initial Value
$C_{eq,tread}$	J/K	50	200	125
$C_{eq,carcass}$	J/K	1000	3000	2000
$h_{tread,amb}$	W/K	10	50	30
$h_{carcass,amb}$	W/K	10	50	30
$h_{tread,carc}$	W/K	20	50	80
$H_{tread,road}$	W/m^2K	2000	4000	3000
λ	no unit	0.4	1	0.7
E_i	no unit	0.01	0.03	0.02

Table 4.3: Bounds of the optimization algorithm

Note that $C_{eq,tread}$ and $C_{eq,carcass}$ are thermal capacities and include the mass,

while references of Table 4.2 provided specific thermal capacities. Because of that, considering the known mass of Continental 205/470 R13 tyre and approximating a ratio of 95%-5% between carcass and tread, initial values of the optimization have been defined.

Four datasets from Tire Test Consortium are used for the parameter estimation: two from pure cornering tests and two from combined (lateral and longitudinal) tests. Being very large, each dataset has been divided in smaller sub-datasets (e.g. Lateral 1A, 1B...), and the optimization algorithm has been run to each of them. Parameter estimation has been performed in the current model, which from now on is called "2DOF EVO", and in the benchmark models "1DOF" and "2DOF". This is done to make performance comparison between them. In the following table 2DOF EVO results are shown in terms of values and mean-squared relative error with respect to measured data:

Sub-Dataset	MRE	$C_{eq,tread}$ [J/K]	$C_{eq,carcass}$ [J/K]	$h_{tread,amb}$ [W/K]	$h_{carcass,amb}$ [W/K]	$h_{tread,carc}$ [W/K]	$H_{tread,road}$ [W/m^2K]	λ [-]	E_x [-]	E_y [-]	E_z [-]
Lateral 1A	2.81%	200	2727	10	10	80	2000	0.481	0.03	0.03	0.03
Lateral 1B	3.45%	200	3000	10	10	80	2000	0.415	0.03	0.03	0.03
Lateral 1C	2.88%	200	2699	10	10	80	2000	0.498	0.03	0.03	0.03
Lateral 2A	3.02%	200	3000	10	10	64.4	2248	0.4	0.03	0.03	0.03
Lateral 2B	2.66%	200	2140	10	10	80	2000	0.422	0.03	0.03	0.03
Lateral 2C	2.47%	200	2203	10	10	80	2000	0.41	0.03	0.03	0.03

Table 4.4: Parameter estimation results (pure lateral)

Sub-Dataset	MRE	$C_{eq,tread}$ [J/K]	$C_{eq,carcass}$ [J/K]	$h_{tread,amb}$ [W/K]	$h_{carcass,amb}$ [W/K]	$h_{tread,carc}$ [W/K]	$H_{tread,road}$ [W/m^2K]	λ [-]	E_x [-]	E_y [-]	E_z [-]
Combined 1A	4.23%	200	1000	10	15.4	80	2000	0.548	0.03	0.018	0.03
Combined 1B	3.48%	200	1017	10	10	80	2000	0.46	0.03	0.01	0.03
Combined 1C	3.56%	200	1002	10	10	80	2000	0.447	0.03	0.01	0.03
Combined 1D	3.19%	200	1000	10	10.5	80	2000	0.446	0.03	0.01	0.03
Combined 2A	4.13%	200	1003	12.1	18.8	80	2000	0.4	0.03	0.01	0.03
Combined 2B	3.92%	200	2228	10.7	12	79.7	2000	0.4	0.03	0.01	0.03
Combined 2C	3.77%	200	3000	10	10	76.5	2000	0.426	0.03	0.01	0.03

Table 4.5: Parameter estimation results (combined drive/brake)

It is possible to see that the optimization algorithm worked well, in fact the MRE of each sub-dataset is very low, about 2-3%. Also, many parameters have been estimated to the same value regardlessly the test performed (e.g. the heat exchange coefficients and $C_{eq,tread}$). The parameters that diverged the most through the sub-datasets are $C_{eq,carcass}$ and E:

- $C_{eq,carcass}$ is sensitive to the test type, since pure cornering tests provide a different result with respect to combined ones.

- E parameters differ too between lateral and combined tests, especially E_y. However, deflection power contribution to the tyre thermal behaviour is minor with respect to the others so different values of E don't cause large differences.

It is very important to analyse also the results obtained about λ. It is a crucial parameter, probably the most important, since it defines the friction power produced by the tyre, which is the most important contribution to the thermal behaviour. Small variations of λ produce big changes in terms of power, because of that the different values obtained in all the sub-datasets may be seen as a bad result. Actually, λ results in almost all simulations to a value inside the bounds, which is a sign that the optimization works very well since it doesn't tend to a value outside the bounds. In fact, with a range of [0.4 1] all the values are about between 0.4 and 0.5. In Figure 4.6 is shown the λ estimation comparison between 2DOF and 2DOF EVO.

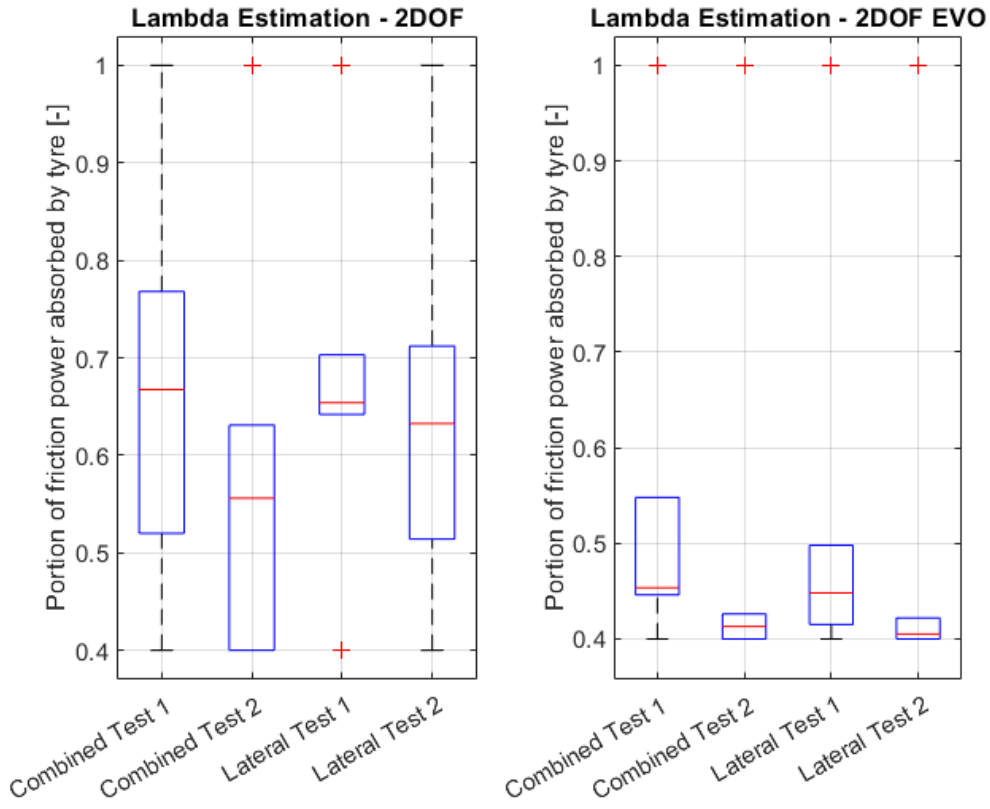

Figure 4.6: Results dispersion of lambda estimation of the two models

The figure contains two box plots: the red/black limits correspond to the optimization bounds. Each column (Combined Test 1,2 and Lateral Test 1,2) corresponds to the results of a single dataset which has been divided in many sub-datasets. The blue boxes contain the optimization results of the sub-datasets, giving the dispersion inside each dataset. It's possible to see that 2DOF model gives a higher dispersion in λ's values, about between 0.5 and 0.75.

As it's shown in Table 4.4 and 4.5, many parameters have been estimated and different results have been obtained according to the subdataset considered. However, to perform model validation, a common set of parameters that works well with every subdataset is needed. Different procedures have been considered, for example using the average of the values obtained in each dataset. But this method didn't work because subdatasets have different lengths (amount of data) so using the average value wouldn't have any meaning. Simply by looking the results of the optimizations, a set of parameters have been found doing trial and error and trying to get the best trade-off among the subdatasets.
This procedure has been applied on benchmark models and 2DOF EVO, the final parameters are reported in Table 4.6:

Parameter	**u.m.**	**1DOF**	**2DOF**	**2DOF EVO**
$C_{eq,tyre}$	J/K	2000	-	-
$C_{eq,tread}$	J/K	-	700	200
$C_{eq,carcass}$	J/K	-	5500	2500
h	W/K	30	-	-
$h_{tread,amb}$	W/K	-	10	10
$h_{carcass,amb}$	W/K	-	22	10
$h_{tread,carc}$	W/K	-	70	80
$H_{tread,road}$	W/m^2K	-	5	2000
λ	no unit	0.75	0.76	0.4
E_x	no unit	-	-	0.02
E_y	no unit	-	-	0.025
E_z	no unit	0.01 (k_r)	0.01 (k_r)	0.03

Table 4.6: Final model parameters

Validation of the models has been performed testing them on the entire datasets (Combined 1/2, Lateral 1/2). Mean squared relative error has been computed, as

in the parameter estimation, obtaining the results shown in Table 4.7 and Figure 4.7.

Dataset	1DOF	2DOF	2DOF-EVO
Combined 1	7.91%	6.40%	5.56%
Combined 2	7.81%	5.48%	6.49%
Lateral 1	6.14%	6.09%	5.59%
Lateral 2	7.57%	6.68%	4.32%

Table 4.7: Mean squared relative error on each dataset

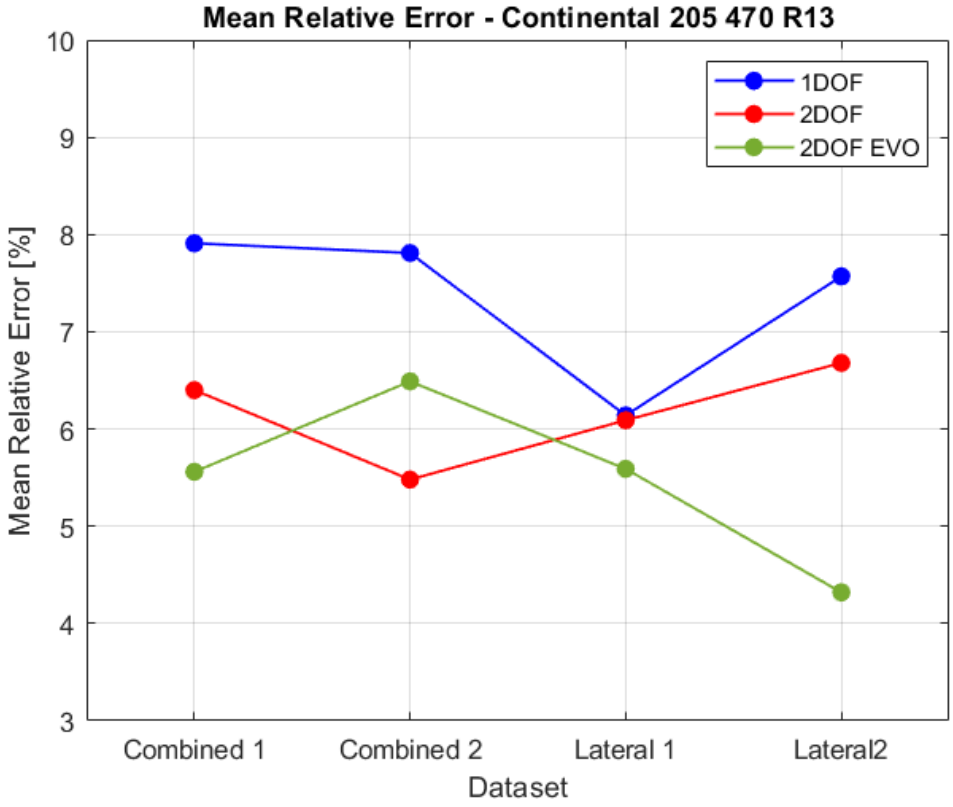

Figure 4.7: Plot of mean squared relative errors on datasets

First, it's possible to see that 1DOF model has the worst performance. This is due mainly to the tyre model, since a single layer has to represent both external and internal layers. In this way a single temperature dynamics becomes not so accurate

as in the 2DOFs. In fact, 2DOF and 2DOF EVO show a better performance than 1DOF because it's possible to represent the lower dynamics of carcass temperature and the higher one of tread, as depicted in Figure 4.8.

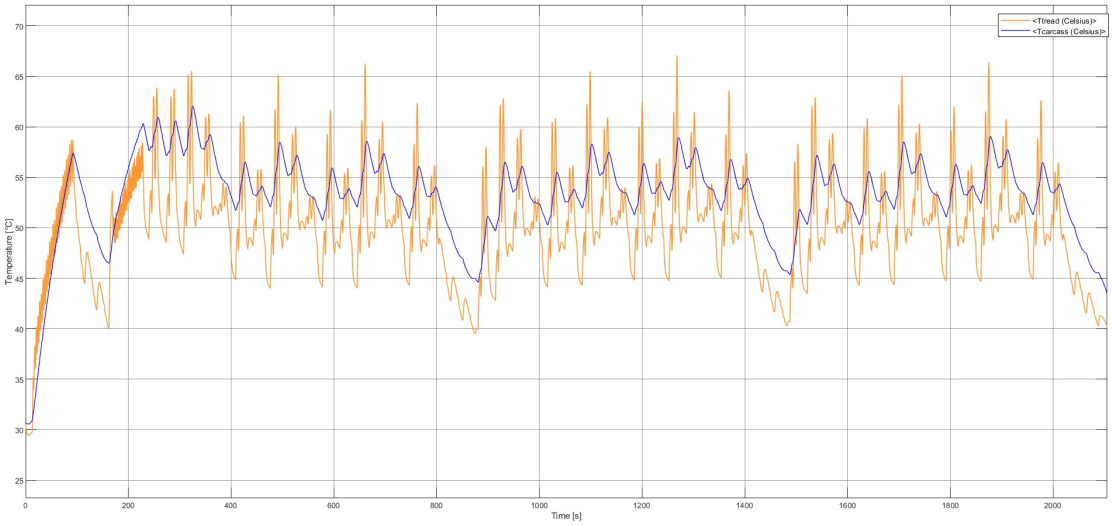

Figure 4.8: Behaviour of tread and carcass temperature in pure cornering test

2DOF EVO model is the one which provides the best performance, with mean squared relative errors around 5%. This confirms that the modelling choices (addition of road conduction and internal deflection) are correct and produce an improvement. 2DOF model still behaves better in Combined 2 dataset but performs worse in the others.

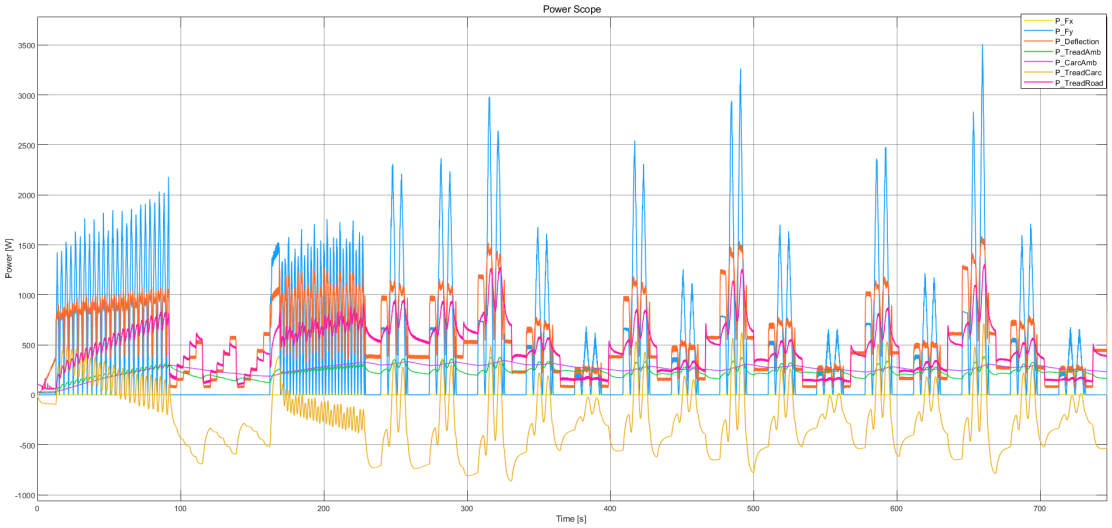

Figure 4.9: Powers exchanged by the tyre in pure cornering test

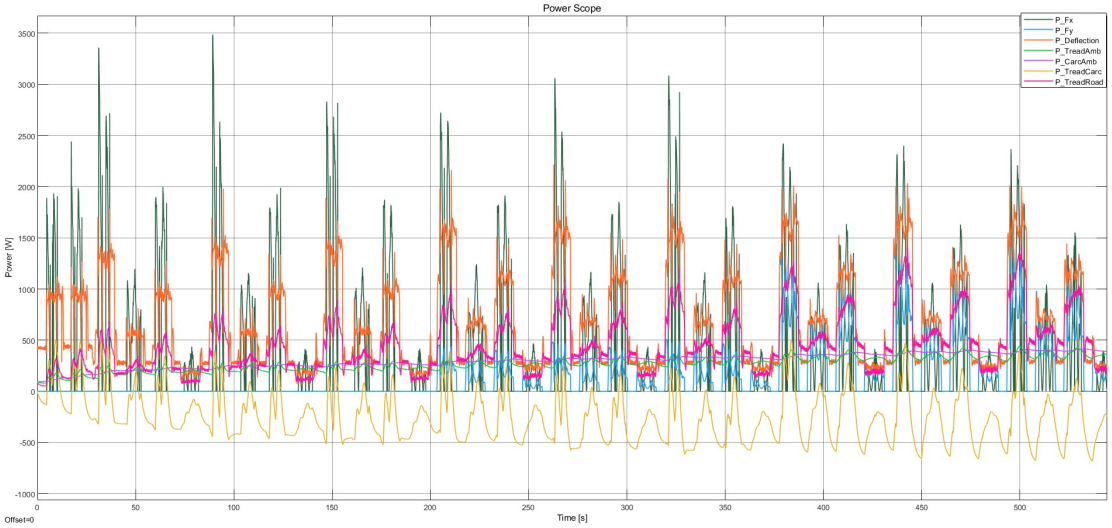

Figure 4.10: Powers exchanged by the tyre in drive/brake combined test

In Figure 4.9 and 4.10 the evolution of powers exchanged by the tyre is shown. This representation is very important to understand what is the contribution of each heat exchange phenomenon. It's possible to see that the most important contribution comes from friction power (blue and dark green lines), this confirms that the correct lambda estimation is a key factor. In Figure 4.9 the friction power comes only from Fy (blue line) since it is a pure cornering test. Tyre deflection energy (orange line) has a lower contribution but not negligible. For what concerns

the heat losses, the highest loss comes from tread-road conduction.
Note that in this image all the powers are represented in absolute value except tread-carcass convection, which is positive when heat is from tread to carcass and negative when vice-versa.

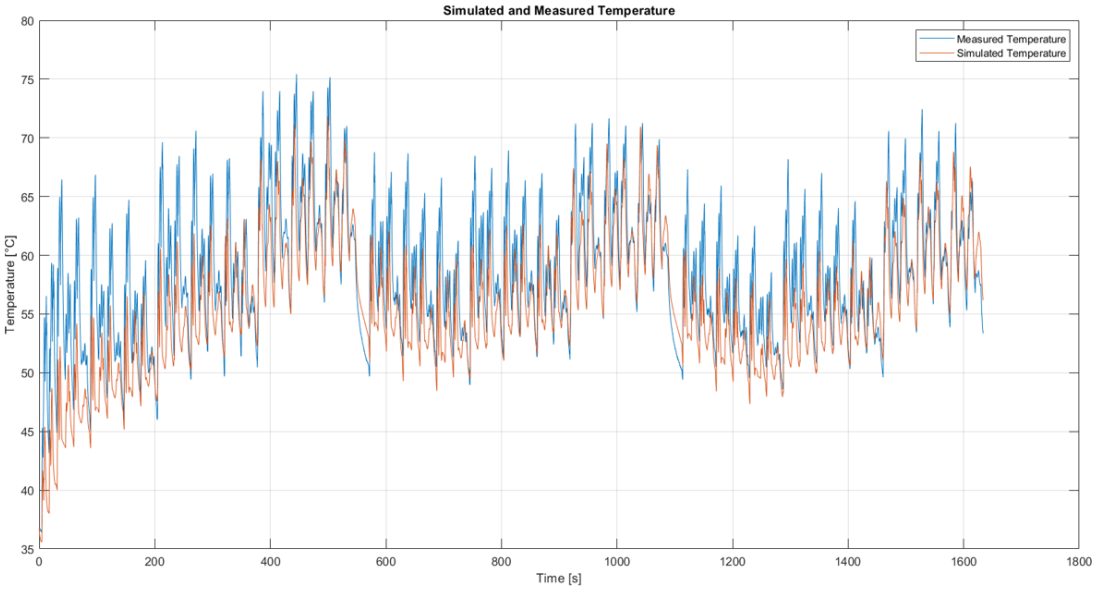

Figure 4.11: Model vs measured temperature in combined test

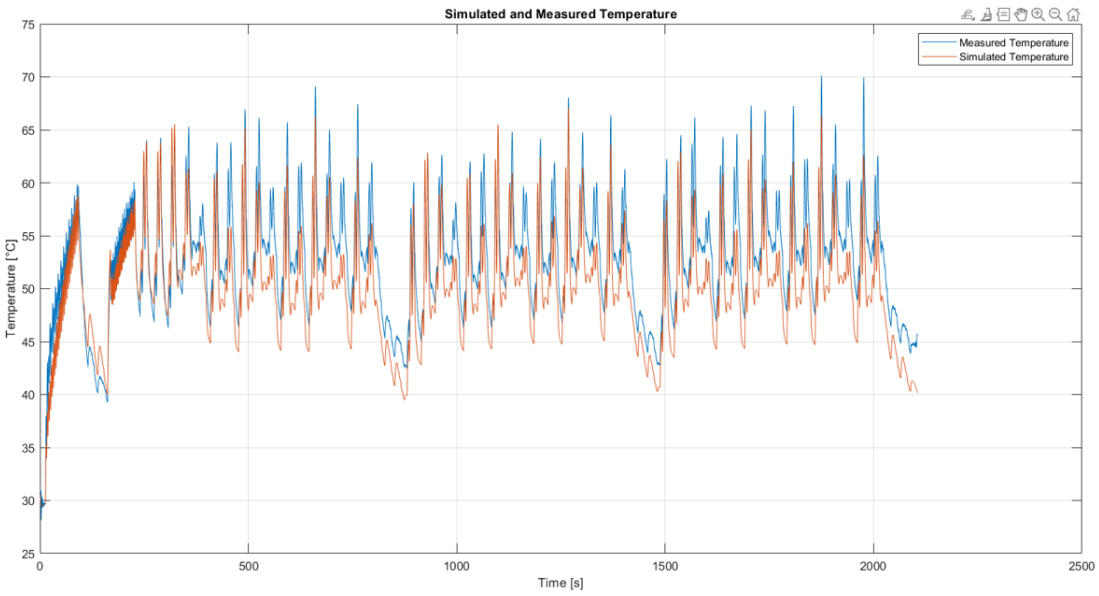

Figure 4.12: Model vs measured in pure cornering test

Figures 4.11 and 4.12 shows a clear view how tread temperature from the model behaves against the one measured from test, and results are satisfying.

4.2.4 Future Improvements

One of the main drawbacks of the proposed thermal model is that in some conditions it underestimates (Figure 4.13) or overestimates (Figure 4.14) the measured temperature.

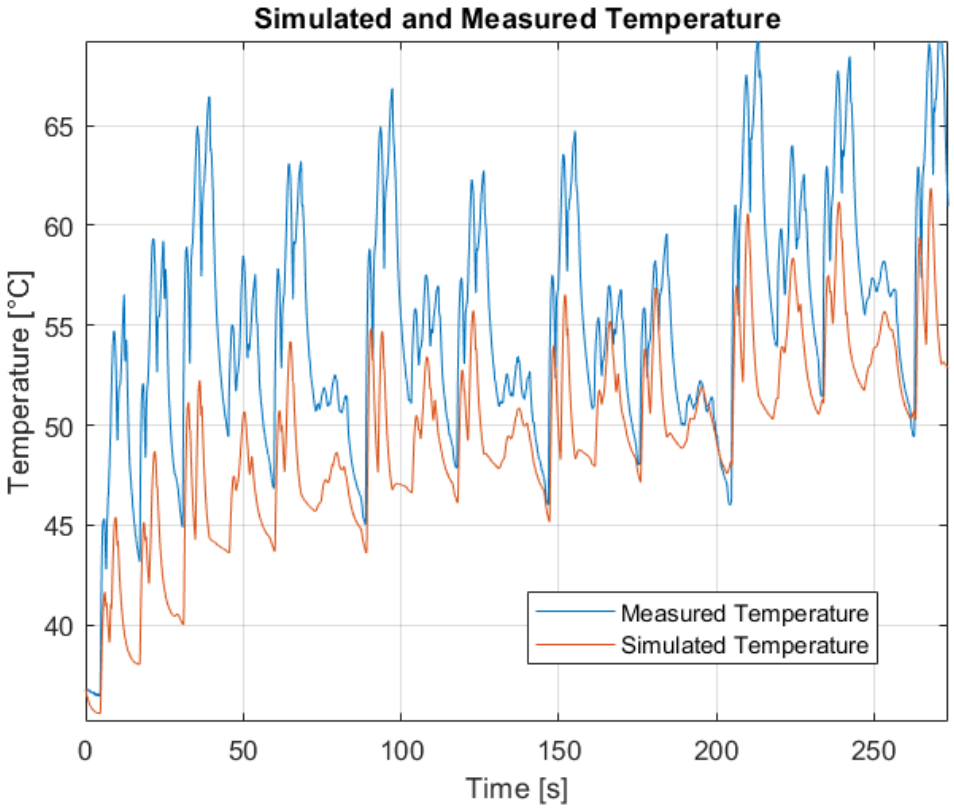

Figure 4.13: Underestimation of tread temperature, combined test

Possible reasons can be:

- Low complexity of the model
- Absence of tyre wear modelling

While the second condition is very difficult to model from a mathematical point of view, the complexity of the model may be increased adding a third degree-of-freedom.

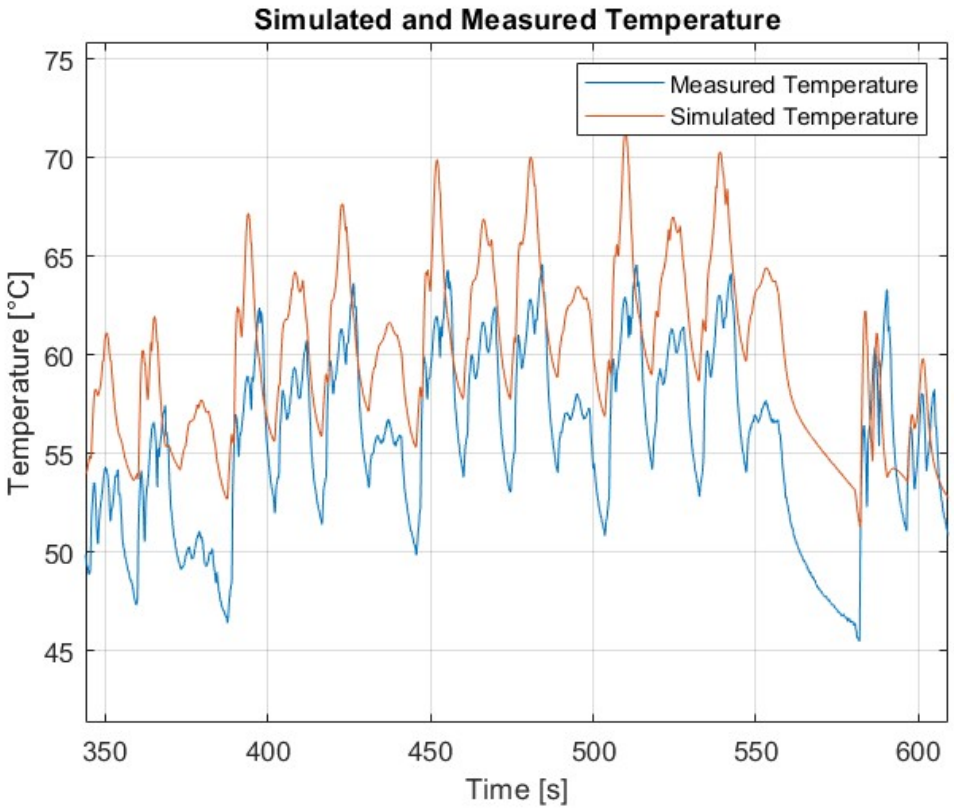

Figure 4.14: Overestimation of tread temperature, combined test

D. P. Kelly and R. S. Sharp proposes in [**6**] a 3DOF thermal model in which tyre is divided in three layers: tread, carcass and inner gas, as in Figure 4.15. In this way a new state is added, T_{gas}, and new thermal coefficients:

- $C_{eq,gas}$
- $H_{carcass,gas}$

This approach hasn't been considered in this project since estimation of pressure and gas temperature is needed, increasing a lot model complexity. Also, 2DOF EVO model provides very good results so a 3DOF model would have added only a small improvement.

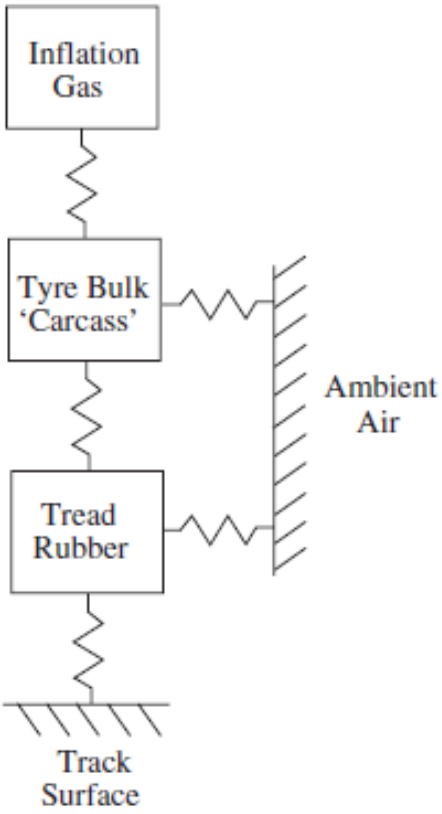

Figure 4.15: 3DOF thermal model schematic

Chapter 5

Adaptive Tyre Model

5.1 Introduction

This chapter shows the adaptive tyre model used to calculate tyre forces. First the Magic Formula tyre model, developed by Pacejka et al. [**11**], is described. This is an empirical model, so its coefficients are fitted using measurement data and the procedure is shown. Then it's explained how the model can be modified, as proposed by Harsh [**12**], to take into account the effects of tyre temperature on the tyre forces production. It's important to consider that Magic Formula is a steady-state tyre model so the obtained forces are for steady-state conditions. An updated fitting procedure is defined with new empirical coefficients related to temperature effects. The coefficients related to Formula SAE tyre Continental 205/470 R13 are fitted and finally, the performance of the adaptive tyre model is compared with measurement data and results are analysed.

5.2 Pacejka's Magic Formula

A widely used semi-empirical tyre model to calculate steady-state tyre force and moment characteristics for use in vehicle dynamics studies is based on the so called Magic Formula. The general form of the function is:

$$y = D\sin[C\arctan Bx - E(Bx - \arctan Bx)] \tag{5.1}$$

$$Y(X) = y(x) + S_v \tag{5.2}$$

$$x = X + S_h \tag{5.3}$$

$Y(X)$ is model output, that can be longitudinal force, lateral force or self-aligning torque. X is model input, that can be slip angle α or longitudinal slip κ. The other coefficients of the function are called:

- B: stiffness factor
- C: shape factor
- D: peak factor
- E: curvature factor
- S_h: horizontal shift
- S_v: vertical shift

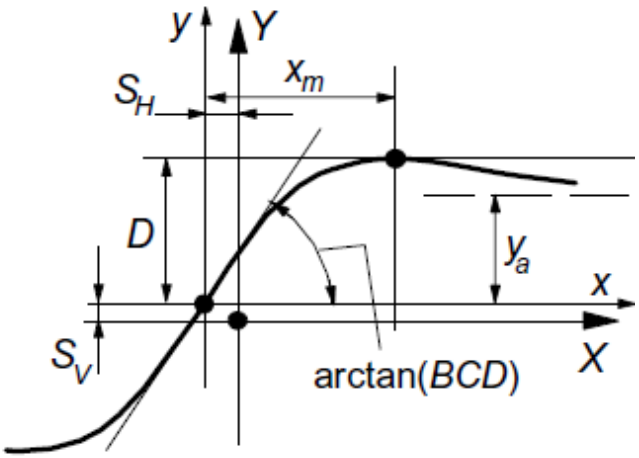

Figure 5.1: Curve produced by the general version of Magic Formula, [**11**]

The Magic Formula $y(x)$ typically produces a curve that passes through the origin $x = y = 0$, reaches a maximum and subsequently tends to a horizontal asymptote. For given values of the coefficients B, C, D and E the curve shows an anti-symmetric shape with respect to the origin. To allow the curve to have an offset with respect to the origin, two shifts S_h and S_v have been introduced.

Magic Formula is a sine formula and its peak value is determined by coefficient D (peak factor). The product BCD corresponds to the slope at the origin (x = y = 0). The shape factor C controls the limits of the range of the sine function, determining the shape of the curve. The stiffness factor B is left to determine the slope at the origin. The curvature factor E is introduced to control the curvature at the peak and at the same time the horizontal position of the peak.

A constant value of the coefficients makes the equation valid for a particular load, camber angle and pressure. Thus, the model is dependent by Fz, γ and p.

In order to affect their performance changes, nominal load, nominal camber and nominal pressure are defined, which performance is known from measurements. Then, from the actual value and the nominal one, deltas are computed:

$$\Delta F_z = \frac{F_z - F_{z0}}{F_{z0}} \tag{5.4}$$

$$\Delta\gamma = \frac{\gamma - \gamma_0}{\gamma_0} \tag{5.5}$$

$$\Delta p = \frac{p - p_0}{p_0} \tag{5.6}$$

These deltas are inside the formulas of previous coefficients, adding their influence on model output.

5.2.1 Tyre Model Fitting to Tyre Data

To resume the previous subchapter, Pacejka's model inputs are:

- κ: longitudinal slip
- α: slip angle
- Fz: vertical load
- γ: camber angle
- p: tyre pressure

However, these are not the only Pacejka's model input: in simulation environment a *.tir* file is used to take into account all the properties of the considered tyre. Tir files contain several empirical coefficients that defines tyre behaviour on forces and moments production capability in all three directions. These coefficients are used with the deltas mentioned before to compute B, C, D, E, S_h, S_v.
Tir files are structured as a ASCII file and are made by the following sections:

- MODEL: contains information about the version of Magic Formula used
- DIMENSION: contains information about tyre dimensions
- OPERATING CONDITIONS: contains nominal temperature and pressure
- INERTIA: contains tyre mass and inertia moments
- VERTICAL: contains vertical load and coefficients about vertical stiffness
- STRUCTURAL: contains information about tyre stiffness and damping

- CONTACT PATCH: contains coefficients to compute contact patch length and width
- SCALING COEFFICIENTS: contains coefficients that are used to scale the outputs according to different operating conditions (e.g. road surface, temperature, wear)
- LONGITUDINAL COEFFICIENTS: contains those that are used to compute Fx
- OVERTURNING COEFFICIENTS: contains those that are used to compute Mx
- LATERAL COEFFICIENTS: contains those that are used to compute Fy
- ROLLING COEFFICIENTS: contains those that are used to compute My
- ALIGNING COEFFICIENTS: contains those that are used to compute Mz
- TURN-SLIP COEFFICIENTS: contains those related to tyre spin effect

```
[LATERAL_COEFFICIENTS]
PCY1                    =2.8811        $Shape factor Cfy for lateral forces
PDY1                    =2.4300        $Lateral friction Muy
PDY2                    =-0.5        $Variation of friction Muy with load
PDY3                    =0.7044        $Variation of friction Muy with squared camber
PEY1                    =1.1747        $Lateral curvature Efy at Fznom
PEY2                    =-0.3180        $Variation of curvature Efy with load
PEY3                    =0.0371        $Zero order camber dependency of curvature Efy
PEY4                    =-0.4523        $Variation of curvature Efy with camber
PEY5                    =27.4710        $Variation of curvature Efy with camber squared
PKY1                    =-45.5567        $Maximum value of stiffness Kfy/Fznom
PKY2                    =2.0599        $Load at which Kfy reaches maximum value
PKY3                    =1.00        $Variation of Kfy/Fznom with camber
PKY4                    =2.00        $Curvature of stiffness Kfy
PKY5                    =-90.00        $Peak stiffness variation with camber squared
PKY6                    =-3.0720        $Fy camber stiffness factor
PKY7                    =0.2593        $Vertical load dependency of camber stiffness
PHY1                    =0.0008        $Horizontal shift Shy at Fznom
PHY2                    =0.0046        $Variation of shift Shy with load
PVY1                    =0.0280        $Vertical shift in Svy/Fz at Fznom
PVY2                    =0.1647        $Variation of shift Svy/Fz with load
PVY3                    =-3.1313        $Variation of shift Svy/Fz with camber
PVY4                    =-3.6745        $Variation of shift Svy/Fz with camber and load
PPY1                    =1.0785        $influence of inflation pressure on cornering stiffness
PPY2                    =2        $influence of inflation pressure on dependency of nominal tyre load on cornering stiffness
PPY3                    =-0.1836        $linear influence of inflation pressure on lateral peak friction
PPY4                    =-0.0503        $quadratic influence of inflation pressure on lateral peak friction
PPY5                    =-0.5753        $Influence of inflation pressure on camber stiffness
```

Figure 5.2: Example of lateral coefficients of a tir file

A main focus is given to longitudinal, overturning, lateral, rolling and aligning coefficients, which are the main responsible for production of tyre force and moments. Since these coefficients are all empirical they have to be fitted starting from measurement data.
The fitting procedure is simply based on an optimization algorithm (nonlinear

least squares method), in which Pacejka's curve is matched to measured data, very similarly to chapter 4. The main problem is that tir coefficients are much more than thermal parameters. Estimating a number of coefficients so large would lead to very poor results. For this reason, fitting is done separately for each output Fx, Fy, Mz, Mx, My.
In Figure 5.2 the lateral coefficients of Continental 205/470 R13 tir file are shown. Looking at the coefficients and their description is essential to understand how the fitting procedure works. It's possible to see that almost all coefficients, except few ones, depend on selected parameters, such as vertical load, camber and inflation pressure.
As it has been described previously in Chapter 3, tyre testing is performed at specific ranges of Fz, γ and p. To each range a nominal value can be referred (e.g. if a Fz range is between 500 N and 700 N, the nominal value of this range is 600 N). In this way it's possible to divide test data in many batches, each one related to a single Fz, camber and pressure range.

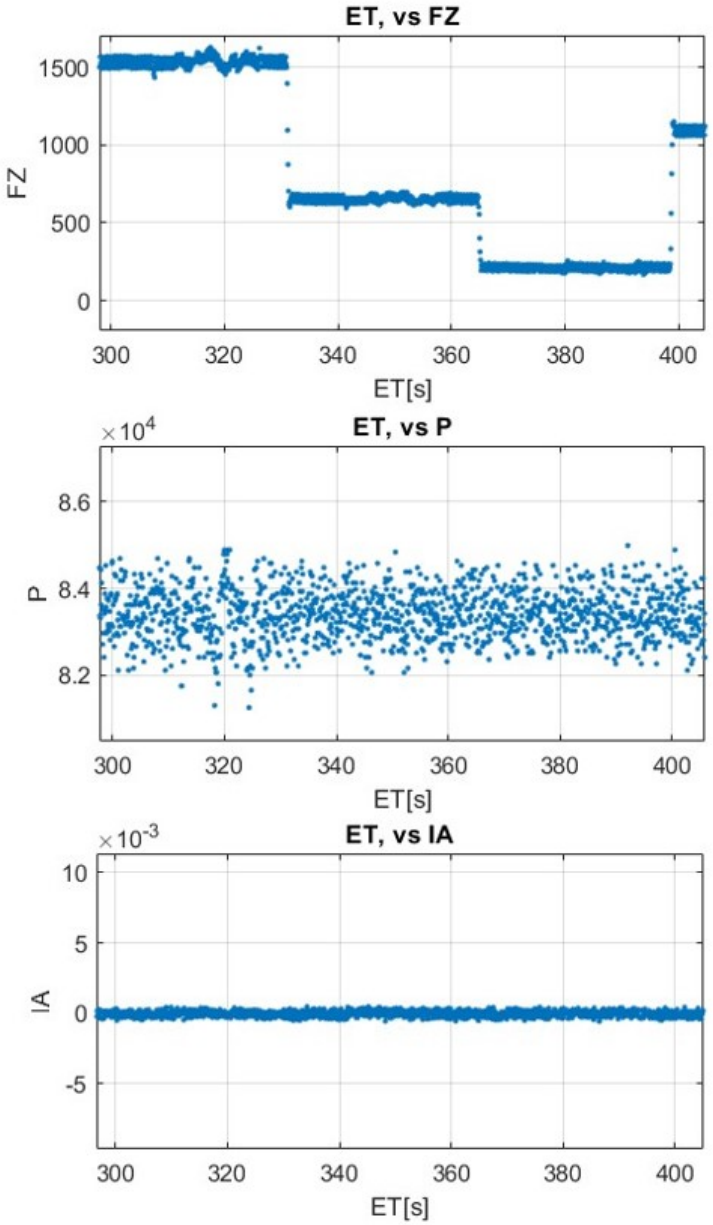

Figure 5.3: Example of how to divide a dataset for fitting

Looking at Figure 5.3, between $Time = 300$ s and $Time = 400$ s, vertical load, camber and pressure have the following behaviour:

- Fz has three different ranges, each with nominal value equal to 1500 N, 600 N, 200 N.

- p is fixed at a range with nominal value equal to 8.3 kPa.
- γ is fixed at a range with nominal value equal 0 deg.

Dividing a dataset in batches means to divide it in time intervals which refer to constant vertical load, camber and pressure. In this case the division, leads to the following batches:

Batch	**Fz**	**Camber**	**Pressure**
1	1500 N	0 deg	8.3 kPa
2	600 N	0 deg	8.3 kPa
3	200 N	0 deg	8.3 kPa

Table 5.1: Division of a dataset according to its nominal values

This division is essential to fit coefficients. As said before, estimating too many coefficients at the same time is difficult. For this reason, for each force/moment output the coefficients are fitted in different steps in the following order:

1. Coefficients depending on nominal vertical load
2. Coefficients depending on vertical load
3. Coefficients depending on camber
4. Coefficients depending on inflation pressure

At each step, coefficients are fitted using batches with all the variables constant except the ones already fitted or that have to be fitted in the current step.
To make it simpler to understand, the batches used at each step have:

- Step 1 - Constant Fz, camber and pressure
- Step 2 - Variable Fz, constant camber and pressure
- Step 3 - Variable Fz and camber, constant pressure
- Step 4 - Variable Fz, camber and pressure

Considering lateral coefficients of Figure 5.2, at each step the following coefficients are fitted:

- Step 1 - PCY1, PDY1, PEY1, PKY1, PKY4, PHY1, PVY1.
- Step 2 - PDY2, PEY2, PKY2, PHY2, PVY2.

- Step 3 - PDY3, PEY3, PEY4, PEY5, PKY3, PKY5, PKY6, PKY7, PVY3, PVY4.
- Step 4 - PPY1, PPY2, PPY3, PPY4, PPY5.

This procedure has to be done for each force/moment coefficients. After all the coefficients are obtained, tir file is ready to be used in the tyre model to view and analyze tyre forces and moments produced. The comparison between a Pacejka's curve coming from tir file and the measured data is shown in Figure 5.4.

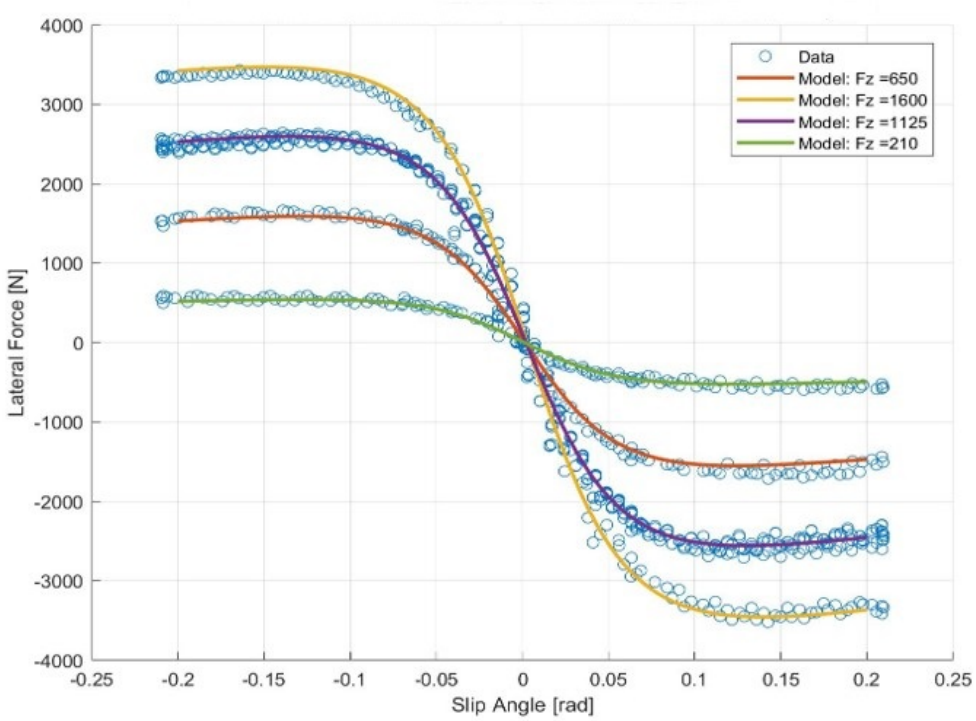

Figure 5.4: Comparison between lateral force produced by MF model with tir file and measured data

5.3 Temperature-Dependent Magic Formula

As it is explained in 2.3.2, temperature has a big influence on tyre force production capability. Pacejka's Magic Formula, despite it is the most used empirical tyre model, doesn't account for this effect. Because of that, a model with effect of temperature is needed and proposed in this chapter with the aim of improving accuracy of model output. The effect of temperature is added following the approach

proposed by Harsh [**12**], in which equations of Magic Formula are modified adding new empirical coefficients that affects stiffness and peak value of the sine curves. In particular, modifications are applied and tested in MATLAB environment using equations from MFEval tool [**13**], which contains all the equation of Magic Formula updated to the most recent version [**14**]. In Appendix A there are all the equations of the model, including the updates to make it temperature dependent.

The influence of temperature on the model works in the same way as the one of vertical load, camber and pressure. In fact, following the approach described in chapter 5.2, a nominal temperature is defined, which performance is known from measured data. Then, actual temperature and nominal one allows to compute δT:

$$\Delta T = \frac{T - T_0}{T_0} \tag{5.7}$$

New empirical coefficients that consider the effect of temperature are added to the tir file and model equations. Four related to lateral behaviour:

- PTY1: influence of tread temperature on cornering stiffness
- PTY2: influence of tread temperature on location of cornering stiffness peak
- PTY3: linear temperature effect on lateral friction
- PTY4: quadratic temperature effect on lateral friction

And four related to longitudinal one:

- PTX1: linear influence of tread temperature on longitudinal slip stiffness
- PTX2: quadratic influence of tread temperature on longitudinal slip stiffness
- PTX3: linear influence of tread temperature on peak longitudinal friction
- PTX4: quadratic influence of tread temperature on peak longitudinal friction

As their description suggests, these coefficients affect cornering stiffness and peak force of the tyre. In fact, they are added to the equations of K, used to compute stiffness factor B, and to peak factor D. Below in black the original equations from MF are showed and in red the modifications related to temperature.

Lateral stiffness factor:

$$K_{y\alpha} = (1 + PTY1\,\Delta T) PKY1\, F_{z0} (1 + PPY1\,\Delta p)(1 - PKY3\,\gamma)$$
$$sin(PKY4\, arctg(\frac{F_z}{F_{z0}(PKY2 + PKY5\,\gamma^2)(1 + PPY2\,\Delta p)(1 + PTY2\,\Delta T)})) \tag{5.8}$$

$$B_y = \frac{K_y}{C_y D_y} \tag{5.9}$$

Longitudinal stiffness factor:

$$K_{x,base} = F_z(PKX1+PKX2\,\Delta F_z)\, e^{(PKX3\,\Delta F_z)}(1+PPX1\,\Delta p+PPX2\,\Delta p^2)LKX \tag{5.10}$$

$$K_x = (1 + PTX1\,\Delta T + PTX2\,\Delta T^2)K_{x,base} \tag{5.11}$$

$$B_x = \frac{K_x}{C_x D_x} \tag{5.12}$$

Lateral peak factor:

$$D_{y,base} = \mu_y F_z \tag{5.13}$$

$$D_y = (1 + PTY3\,\Delta T + PTY4\,\Delta T^2)D_{y,base} \tag{5.14}$$

Longitudinal peak factor:

$$D_{x,base} = \mu_x F_z \tag{5.15}$$

$$D_x = (1 + PTX3\,\Delta T + PTX4\,\Delta T^2)D_{x,base} \tag{5.16}$$

As it is mentioned in section 5.2.1, tir coefficients have to be fitted to experimental data, this also applies for temperature ones. An updated fitting procedure, with a further step with respect of the previous one, is proposed:

- Step 1 - Constant Fz, camber and pressure and temperature
- Step 2 - Variable Fz, constant camber and pressure and temperature
- Step 3 - Variable Fz and camber, constant pressure and temperature
- Step 4 - Variable Fz, camber and pressure, constant temperature
- Step 5 - Variable Fz, camber and pressure and temperature

In the final step the optimization algorithm estimates PTY1, PTY2, PTY3, PTY4 related to F_y and PTX1, PTX2, PTX3, PTX4 for what concerns F_x. An example related to lateral fitting steps is shown below:

- Step 1 - PCY1, PDY1, PEY1, PKY1, PKY4, PHY1, PVY1.
- Step 2 - PDY2, PEY2, PKY2, PHY2, PVY2.

- Step 3 - PDY3, PEY3, PEY4, PEY5, PKY3, PKY5, PKY6, PKY7, PVY3, PVY4.

- Step 4 - PPY1, PPY2, PPY3, PPY4, PPY5.

- Step 5 - PTY1, PTY2, PTY3, PTY4.

In this way the Adaptive Magic Formula takes as new input tyre surface temperature.
Appendix A contains the MATLAB function code of the Adaptive Tyre model, including all the equations to compute longitudinal and lateral force with the modifications to make it temperature-dependent.

5.3.1 Results

During the optimization phase, bounds of all coefficients are set to the range [-5 5] to avoid large values, but the optimized values are all inside this interval so it's irrelevant. The results of the optimization, related to Continental specification, are shown in Table 5.2.

Coefficient	**Value**
PTY1	-0.72506
PTY2	-1.5951
PTY3	-0.02659
PTY4	-1

Table 5.2: Temperature lateral coefficients of Continental 205/470 R13 obtained from data fitting

Coefficients fitting has been possible because TTC test data have been measured at different temperatures. Filtering the data according to vertical load, camber and pressure, it's possible to see how temperature affects tyre performance. In Figure 5.5 normalized lateral force (NFY) is plotted against side slip angle. Points have different colour depending by the temperature. It's easy to see that if temperature is too hot (red) NFY decreases, the same goes if temperature is too cold, confirming the parabolic trend of the temperature operating window.

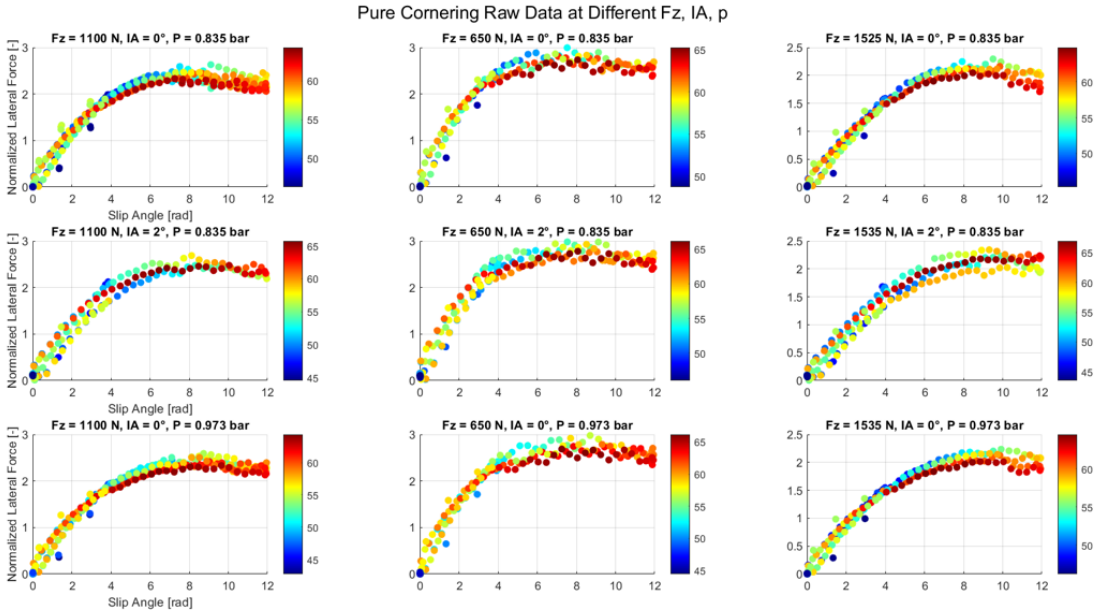

Figure 5.5: Raw data at different F_z, γ, p

A clear view of results provided by the Adaptive Magic Formula is shown in Figure 5.6, 5.7 and 5.8. At fixed F_z, γ and p the model plots different curves at different temperature inputs. It is possible to see in all figures the performance decay at hotter temperatures (e.g. 65 °C). Due to lack of available data in the datasets only a small range of temperature (about [50 65] °C) is analyzed, however results are very good.

The main drawback of lateral performance of the model is related to the bad quality of TTC datasets at variable camber. As it's possible to see in Figure 5.9, varying camber the influence of temperature becomes strange. In fact, the coldest points provide both the worst and best performance, with the hottest in the middle, which is not correct. In fact, even if camber is not null, the temperature operating window would still remains parabolic. For this reason, this model is not tuned at different values of camber.

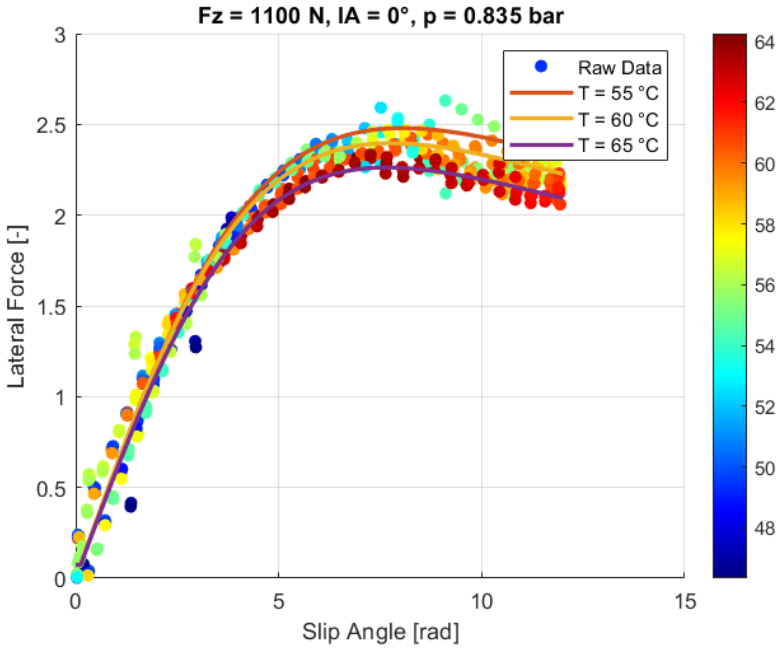

Figure 5.6: Comparison between adaptive Magic Formula's curve and raw data

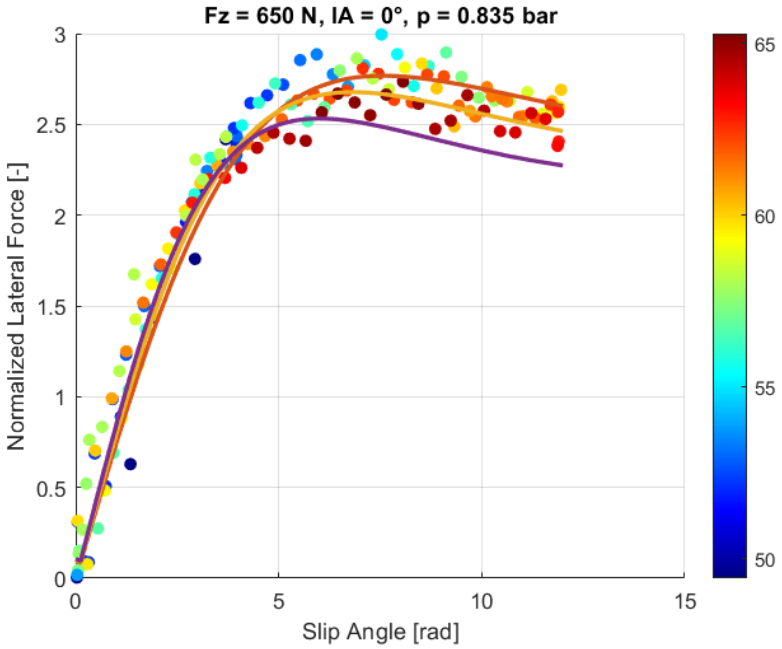

Figure 5.7: Comparison between adaptive Magic Formula's curve and raw data

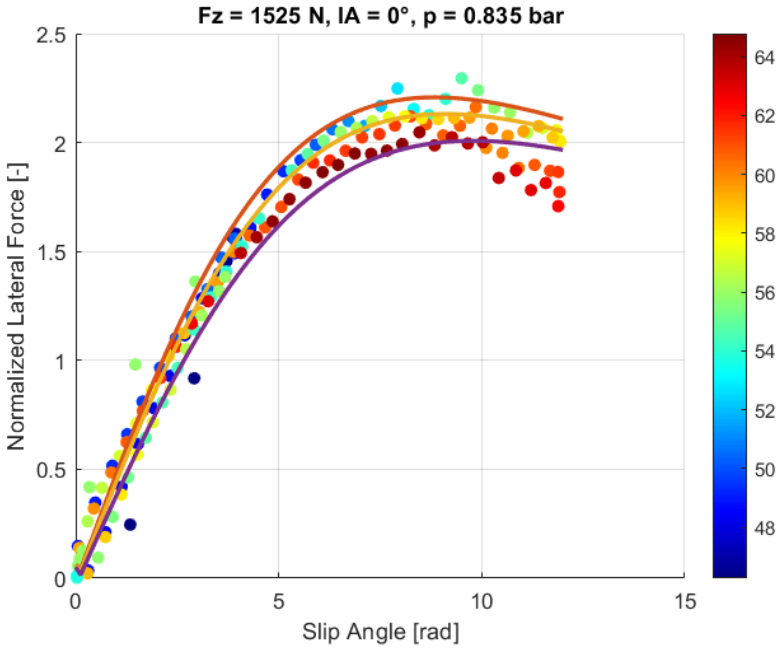

Figure 5.8: Comparison between adaptive Magic Formula's curve and raw data

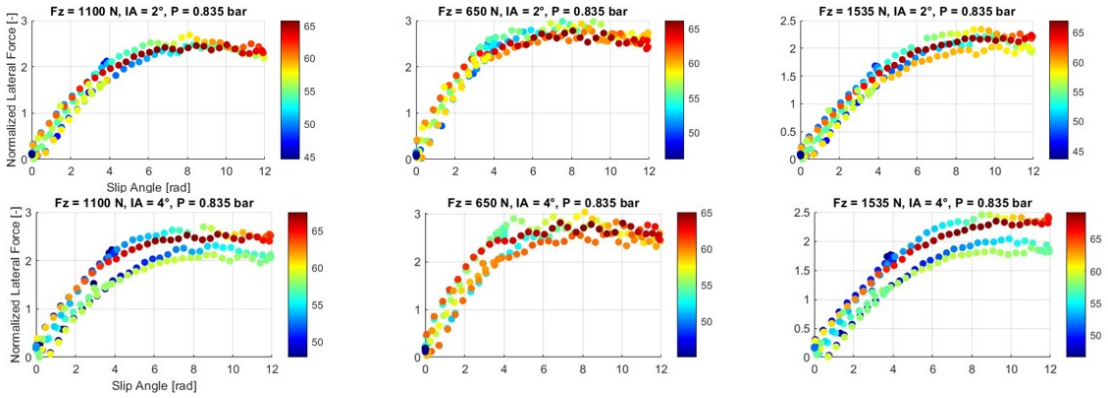

Figure 5.9: Raw data at different F_z, γ, p, focus on camber variation

Performance of the Adaptive Magic Formula is compared to the standard's one. A mean squared relative error is computed, as in Chapter 4, between the force estimated by the model and the one from Calspan measured data. The mean squared relative error on pure cornering dataset is shown below. It's possible to see that the Adaptive Magic Formula reduces well the error of almost -2%. In fact, as it's possible to see in Figure 5.10 and 5.11, which refer to the forces measured in pure cornering, standard Magic Formula overestimate the lateral force, while the

modified (adaptive) one is more accurate.

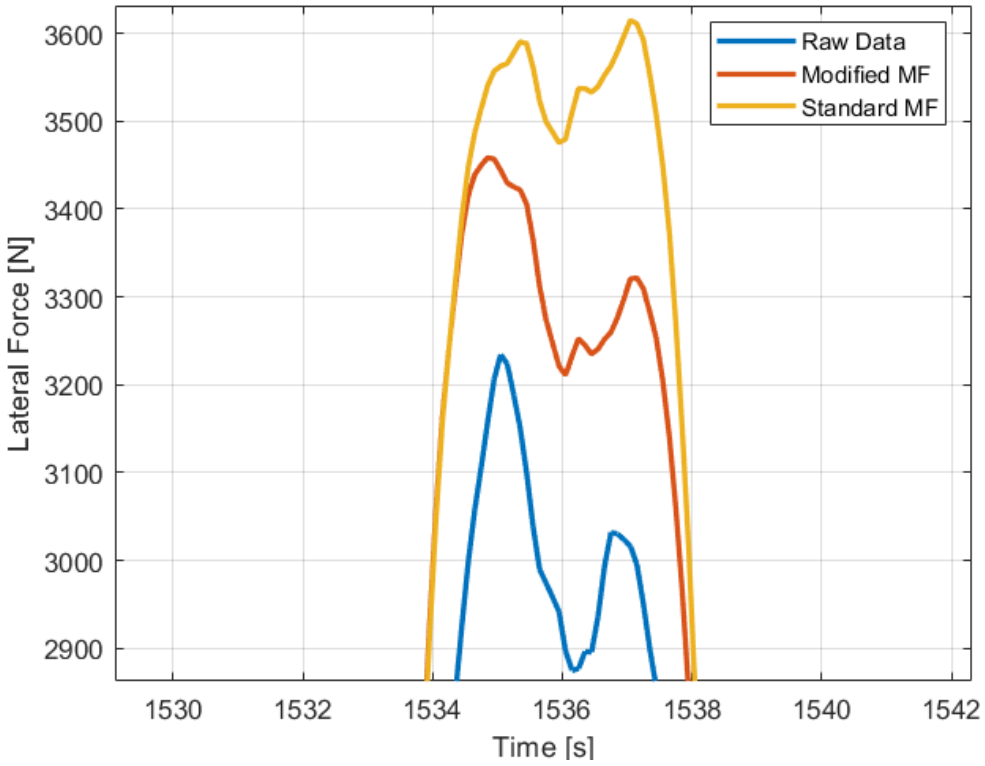

Figure 5.10: Comparison between modified and standard Magic Formula at vertical load $F_z = 1500$ N

Model	Mean Squared Relative Error
Standard MF	10.30%
Adaptive MF	8.61% (-1.7%)

Table 5.3: Estimation errors on measured data from pure cornering test

In Figure 5.12 the error evolution through the dataset is shown. In this picture the error is cumulative, therefore at each time instant the error is summed with those at the previous ones. It's clear that during the test the error difference between two models increases demonstrating that the Adaptive Magic Formula has the best performance.

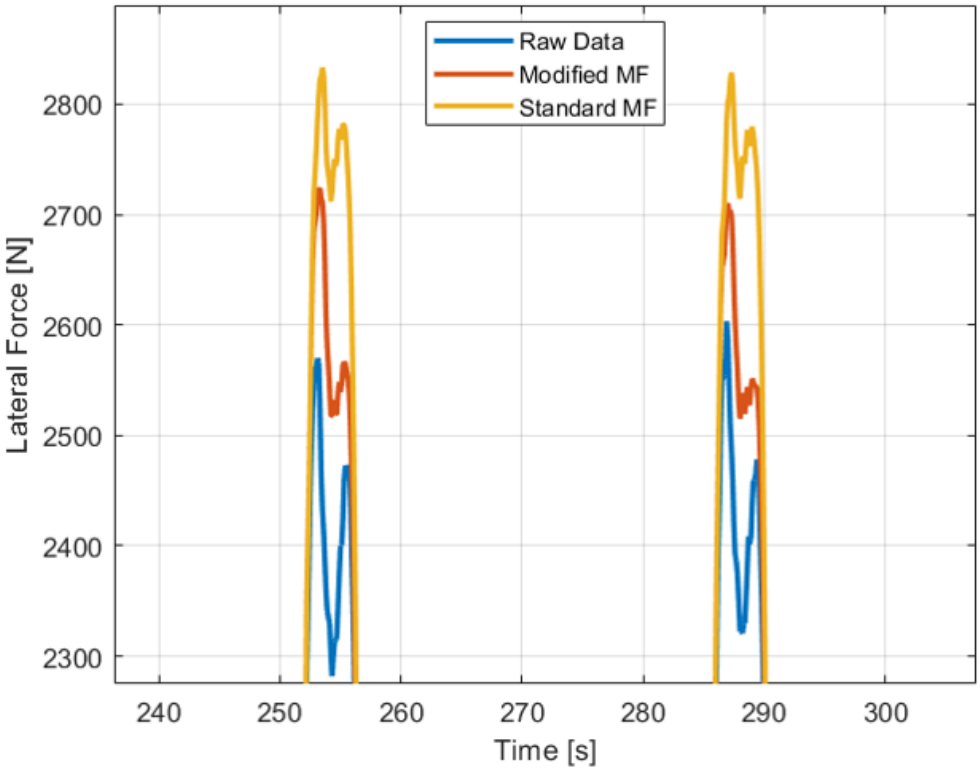

Figure 5.11: Comparison between modified and standard Magic Formula at vertical load $F_z = 1100$ N

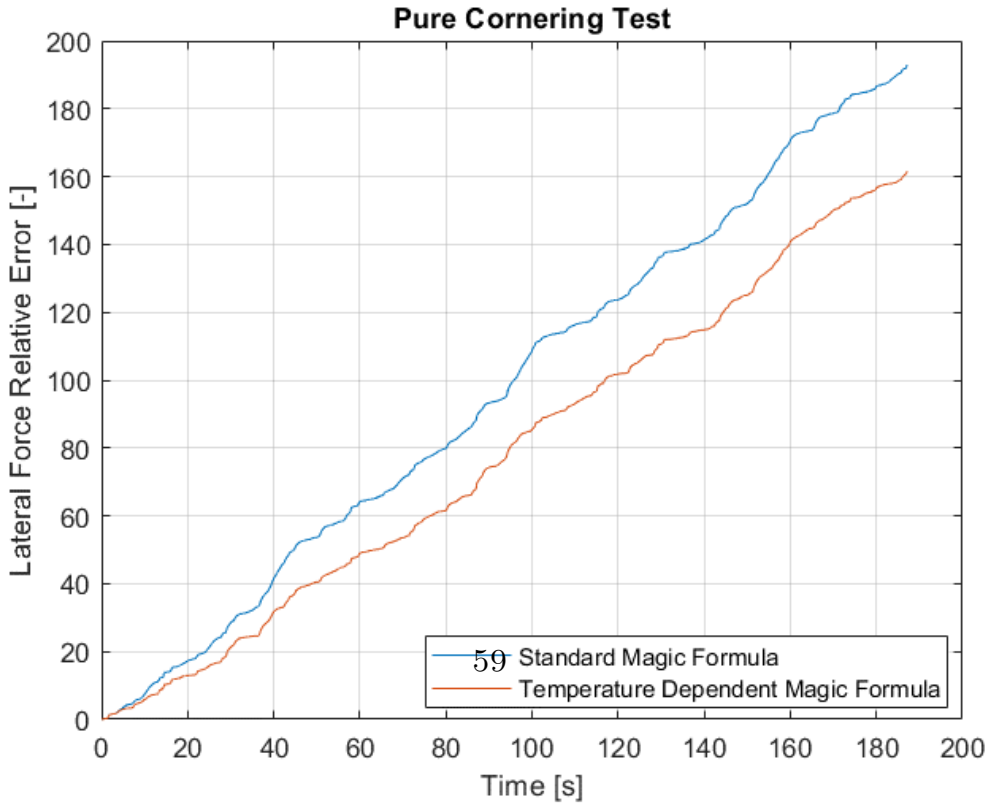

Figure 5.12: Cumulative lateral error between modified and standard Magic Formula

The same procedure has been carried on for longitudinal force too, using Continental 205/470 R13 drive/brake test from TTC.

Coefficient	Value
PTX1	-2.065
PTX2	8.2877
PTX3	-0.50615
PTX4	2.0297

Table 5.4: Temperature longitudinal coefficients of Continental 205/470 R13 obtained from data fitting

In Figure 5.13 the normalized longitudinal force (NFX) is plotted at fixed vertical load, camber and pressure varying the colour according to the temperature, as done for pure cornering test. In this case drive/brake test provides much less data than pure cornering one, and it's evident that a trend depending from temperature, like in Figure 5.8, is very difficult to be defined. Because of that, performance of the model in longitudinal behaviour is not as good as in lateral.

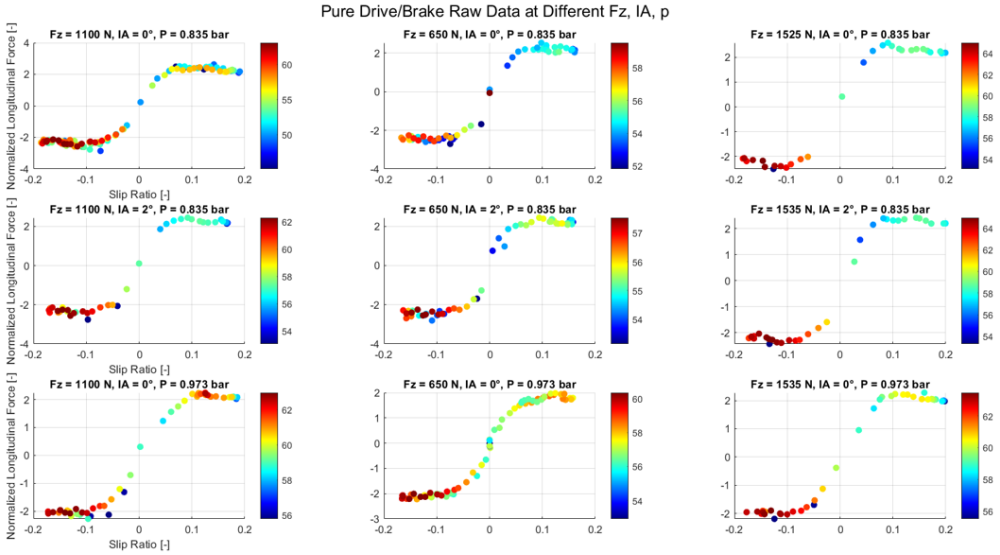

Figure 5.13: Raw data of drive/brake test at different F_z, γ, p

However, there is a small improvement with respect to standard Magic Formula, as seen in examples of Figures 5.14 and 5.15.

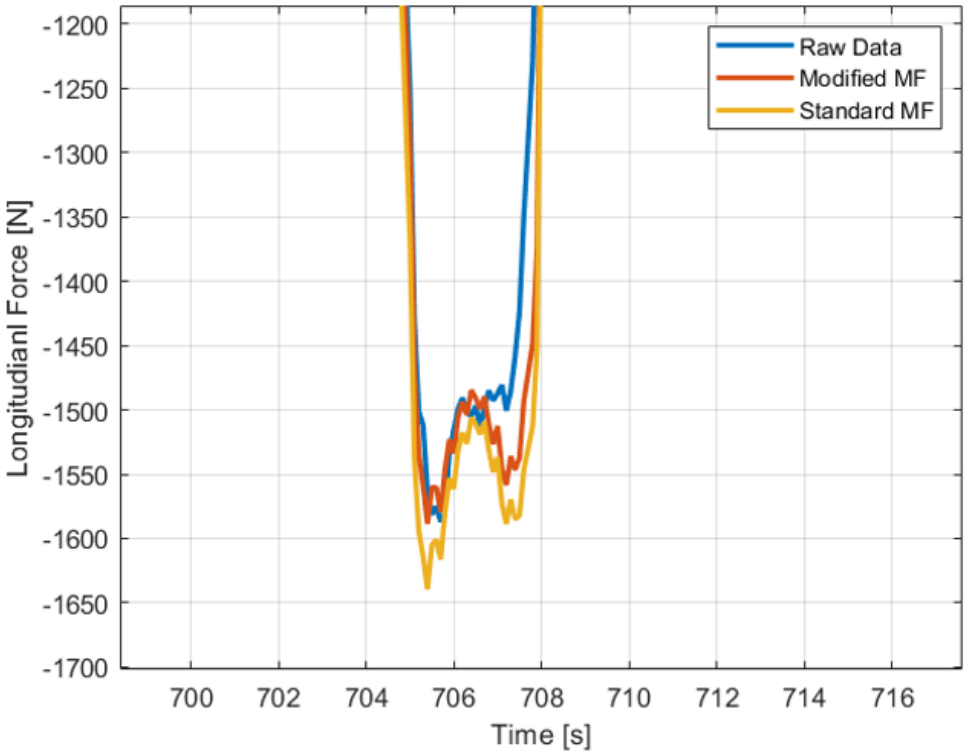

Figure 5.14: Comparison between modified and standard Magic Formula at vertical load $F_z = 650$ N (brake)

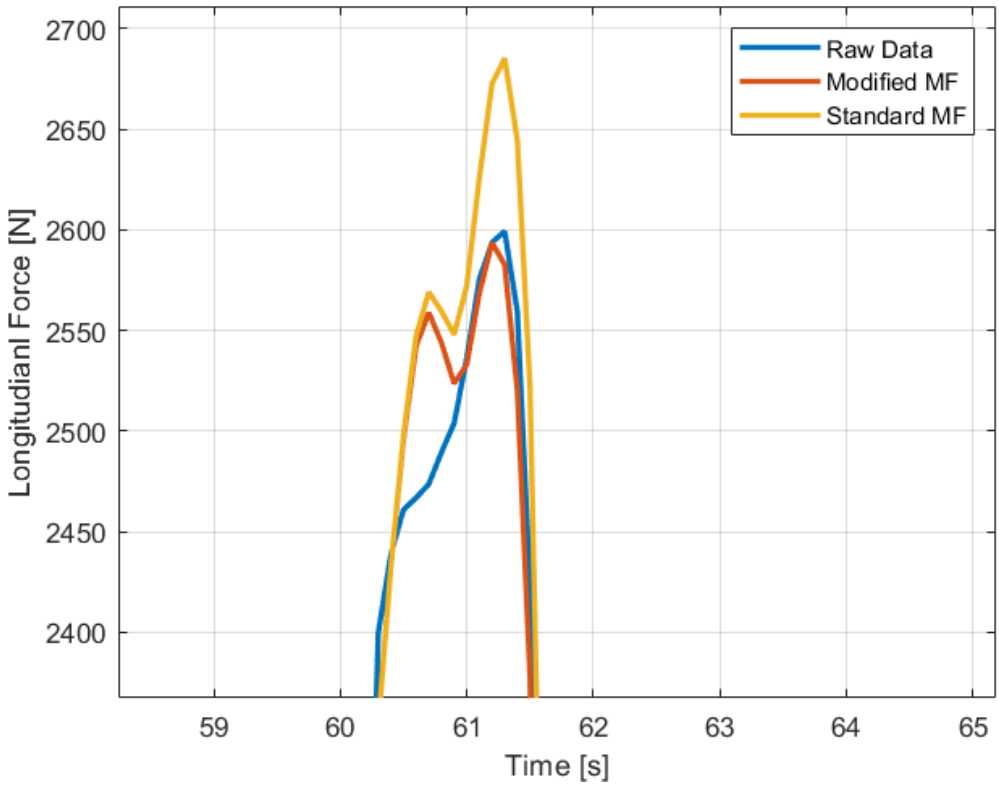

Figure 5.15: Comparison between modified and standard Magic Formula at vertical load $F_z = 1100$ N (drive)

Also, measuring the mean squared relative error of the standard model and the adaptive one against measured data, the temperature dependence improves slightly model accuracy.

Model	Mean Squared Relative Error
Standard MF	7.48%
Adaptive MF	6.93% (-0.55%)

Table 5.5: Estimation errors on measured data from drive/brake test

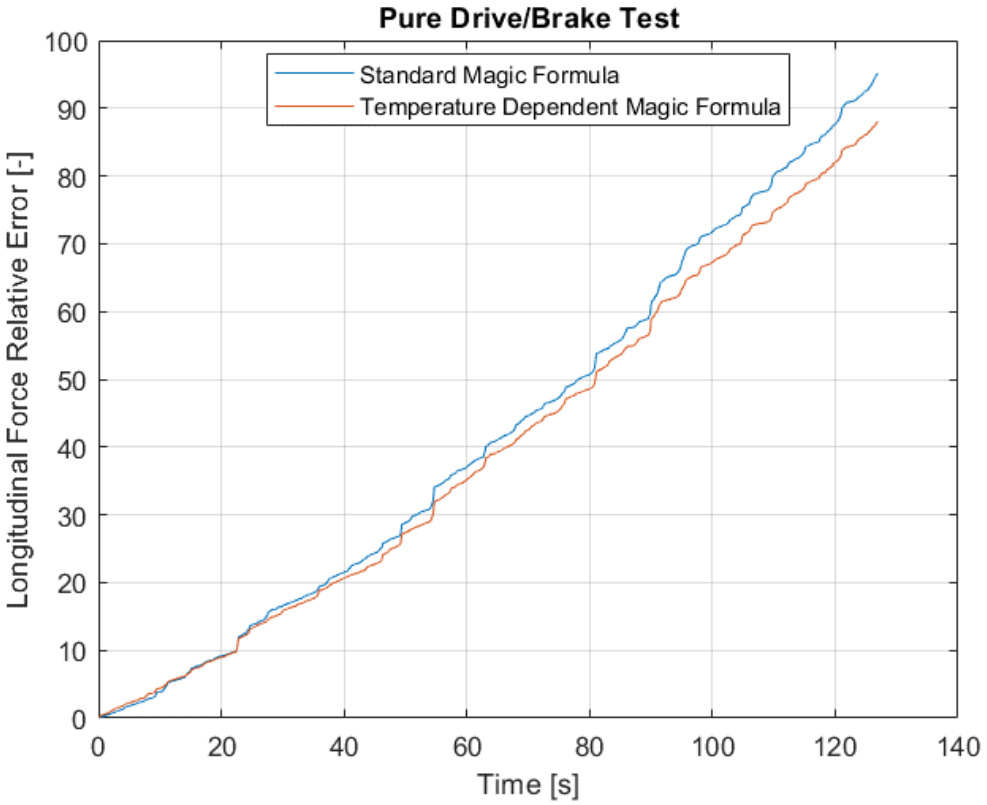

Figure 5.16: Cumulative longitudinal error between modified and standard Magic Formula

5.4 Future Improvements

The results provided by the Adaptive Magic Formula are optimal but they still can be improved. The main limit of model calibration on TTC data is the quality of the datasets. In particular camber sensitivity in pure cornering test on one side and lack of longitudinal data on the other don't allow to improve largely the accuracy with respect to the standard Magic Formula. Squadra Corse's approach for the upcoming future is to feed the model with data from tests on track. The aim is to reproduce the inputs/outputs of a flat trac tests equipping the vehicle with mechanical and thermal sensors. The following procedure would be adopted:

- Equip the vehicle with suspension with strain gauges, measuring the forces at suspension arms and computing from them the forces at the contact patch.
- Mount thermal sensors: infrared sensors to measure tread temperature and TPMS (tyre pressure monitoring system) to measure inner temperature and

pressure of the tyre.

- Measuring tyre side slip angle from vehicle side slip angle estimator already validated with sensors.

In this way the adaptive tyre model would be calibrated on vehicle model and real road surface. The final aim of the model (temperature estimator and adaptive tyre model) is to implement it in vehicle control systems. The system would work in the following way: contact patch forces and slip velocities are used to estimate tyre temperature, which is used as input, together with α, p and F_z, to measure tyre forces F_x and F_y. F_x and F_y allow then to compute tread temperature repeating the loop. Being contact patch forces inputs of many control systems of the car, such as traction control and torque vectoring, a more accurate estimation of them, improved by adding the effect of temperature, would improve the control system performance and overall vehicle one.

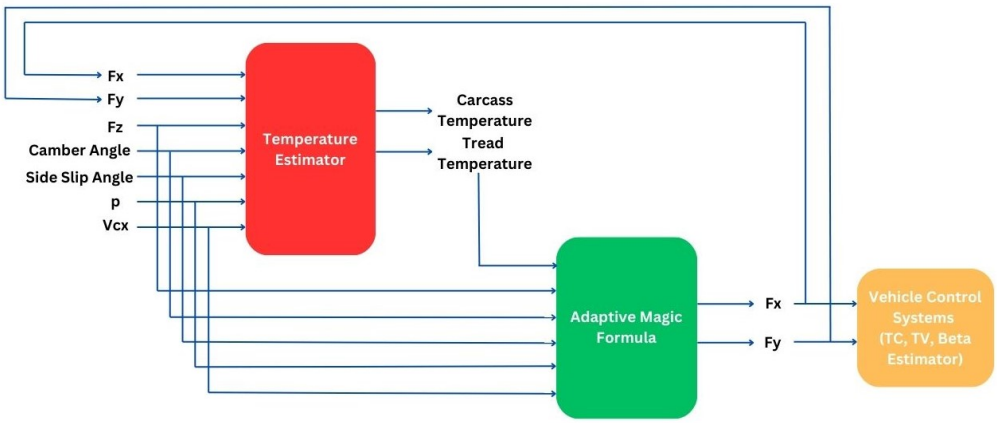

Figure 5.17: Overall scheme of the tyre model

Chapter 6

Conclusions

In this Master's thesis the subject of tyre modelling has been explored deeply, showing first the difficult of tyre models to determine tyre forces, then that the most common tyre models don't account the effect of temperature, which is although a very important parameter that affects tyre performance. A new approach of tyre model has been proposed and its methodology described in detail: estimation of tyre temperature with a lumped parameter model and tyre forces with an adaptive version of Magic Formula. Model has been fitted and tested from flat trac data of a Formula Student tyre (Continental 205/470 R13) and the results are very encouraging. Temperature estimator computes temperature with an error around 5-6% and the adaptive tyre model improves the accuracy, in particular of lateral forces, with respect to the default Magic Formula. This has confirmed that temperature is a key parameter to include in a tyre model and increase its performance. Outputs of the model can be improved way more, and more importantly, calibrated to the real vehicle testing it on track with sensors and collecting a larger amount of data. Once the model is tuned on Squadra Corse's vehicle, it can be used for its final purpose: improve forces estimation and finally control systems and vehicle performance.

Appendix A

Adaptive MF Tyre Model

```
function output = MF_EVO(ParameterSet,INPUTS)

% Unpack INPUTS

Fz = INPUTS(:,1);
kappa = INPUTS(:,2);
alpha = INPUTS(:,3);
gamma = INPUTS(:,4);
Vx = INPUTS(:,5);
p = INPUTS(:,6);
T = INPUTS(:,7);

gamma(:)=deg2rad(gamma(:)); % Conversion to [rad]
alpha(:)=deg2rad(alpha(:)); % Conversion to [rad]
%p(:)=p(:)*10^5; % Conversion to [Pa]
Vcx = Vx;

% Note that all the equation references in this function are related
    to
% Hans B. Pacejka (2006), Tyre and Vehicle Dynamics, 2nd Edition

% Unpack ParameterSet
V0 = ParameterSet.LONGVL;    % Nominal speed
pi0 = ParameterSet.NOMPRES; % Nominal tyre inflation pressure
Fz0 = ParameterSet.FNOMIN;  % Nominal wheel load
T0 = ParameterSet.NOMTEMP; % Nominal tread temperature

LMUV = 0; % Scale factor with slip speed Vs decaying friction

% [SCALING_COEFFICIENTS]
LFZO    = ParameterSet.LFZO;    % Scale factor of nominal (rated) load
```

```
31 LCX     = ParameterSet.LCX ; % Scale factor of Fx shape factor
32 LMUX    = ParameterSet.LMUX;   % Scale factor of Fx peak friction
       coefficient
33 LEX     = ParameterSet.LEX ; % Scale factor of Fx curvature factor
34 LKX     = ParameterSet.LKX ; % Scale factor of Fx slip stiffness
35 LHX     = ParameterSet.LHX ; % Scale factor of Fx horizontal shift
36 LVX     = ParameterSet.LVX ; % Scale factor of Fx vertical shift
37 LCY     = ParameterSet.LCY   ; % Scale factor of Fy shape factor
38 LMUY    = ParameterSet.LMUY;   % Scale factor of Fy peak friction
       coefficient
39 LEY     = ParameterSet.LEY   ; % Scale factor of Fy curvature factor
40 LKY     = ParameterSet.LKY   ; % Scale factor of Fy cornering
       stiffness
41 LHY     = ParameterSet.LHY   ; % Scale factor of Fy horizontal shift
42 LVY     = ParameterSet.LVY   ; % Scale factor of Fy vertical shift
43 LKYC    = ParameterSet.LKYC  ; % Scale factor of camber force
       stiffness
44 LKY     = ParameterSet.LKY ; % Scale factor of Fy cornering stiffness
45 LTR     = ParameterSet.LTR ; % Scale factor of peak of pneumatic trail
46 LRES    = ParameterSet.LRES; % Scale factor for offset of residual
       torque
47 LKZC    = ParameterSet.LKZC; % %Scale factor of camber torque
       stiffness
48 LXAL    = ParameterSet.LXAL ; % Scale factor of alpha influence on Fx
49 LYKA    = ParameterSet.LYKA  ; % Scale factor of alpha influence on Fx
50 LVYKA   = ParameterSet.LVYKA ; % Scale factor of kappa induced Fy
51
52 % [LONGITUDINAL_COEFFICIENTS]
53 PCX1 =   ParameterSet.PCX1;   %Shape factor Cfx for longitudinal force
54 PDX1 =   ParameterSet.PDX1;   %Longitudinal friction Mux at Fznom
55 PDX2 =   ParameterSet.PDX2;   %Variation of friction Mux with load
56 PDX3 =   ParameterSet.PDX3;   %Variation of friction Mux with camber
57 PEX1 =   ParameterSet.PEX1;   %Longitudinal curvature Efx at Fznom
58 PEX2 =   ParameterSet.PEX2;   %Variation of curvature Efx with load
59 PEX3 =   ParameterSet.PEX3;   %Variation of curvature Efx with load
       squared
60 PEX4 =   ParameterSet.PEX4;   %Factor in curvature Efx while driving
61 PKX1 =   ParameterSet.PKX1;   %Longitudinal slip stiffness Kfx/Fz at
       Fznom
62 PKX2 =   ParameterSet.PKX2;   %Variation of slip stiffness Kfx/Fz with
        load
63 PKX3 =   ParameterSet.PKX3;   %Exponent in slip stiffness Kfx/Fz with
       load
64 PHX1 =   ParameterSet.PHX1;   %Horizontal shift Shx at Fznom
65 PHX2 =   ParameterSet.PHX2;   %Variation of shift Shx with load
66 PVX1 =   ParameterSet.PVX1;   %Vertical shift Svx/Fz at Fznom
67 PVX2 =   ParameterSet.PVX2;   %Variation of shift Svx/Fz with load
68 PPX1 =   ParameterSet.PPX1;   %linear influence of inflation pressure
       on longitudinal slip stiffness
```

```
69 PPX2 =  ParameterSet.PPX2;  %quadratic influence of inflation
       pressure on longitudinal slip stiffness
70 PPX3 =  ParameterSet.PPX3;  %linear influence of inflation pressure
       on peak longitudinal friction
71 PPX4 =  ParameterSet.PPX4;  %quadratic influence of inflation
       pressure on peak longitudinal friction
72 PTX1 =  ParameterSet.PTX1;  %linear influence of tread temperature
       on longitudinal slip stiffness
73 PTX2 =  ParameterSet.PTX2;  %quadratic influence of tread
       temperature on longitudinal slip stiffness
74 PTX3 =  ParameterSet.PTX3;  %linear influence of tread temperature
       on peak longitudinal friction
75 PTX4 =  ParameterSet.PTX4;  %quadratic influence of tread
       temperature on peak longitudinal friction
76 RBX1 =  ParameterSet.RBX1; %Slope factor for combined slip Fx
       reduction
77 RBX2 =  ParameterSet.RBX2; %Variation of slope Fx reduction with
       kappa
78 RBX3 =  ParameterSet.RBX3; %Influence of camber on stiffness for Fx
       combined
79 RCX1 =  ParameterSet.RCX1; %Shape factor for combined slip Fx
       reduction
80 REX1 =  ParameterSet.REX1; %Curvature factor of combined Fx
81 REX2 =  ParameterSet.REX2; %Curvature factor of combined Fx with load
82 RHX1 =  ParameterSet.RHX1; %Shift factor for combined slip Fx
       reduction
83
84 % [LATERAL_COEFFICIENTS]
85 PCY1 =  ParameterSet.PCY1   ; %Shape factor Cfy for lateral forces
86 PDY1 =  ParameterSet.PDY1   ; %Lateral friction Muy
87 PDY2 =  ParameterSet.PDY2   ; %Variation of friction Muy with load
88 PDY3 =  ParameterSet.PDY3   ; %Variation of friction Muy with squared
       camber
89 PEY1 =  ParameterSet.PEY1   ; %Lateral curvature Efy at Fznom
90 PEY2 =  ParameterSet.PEY2   ; %Variation of curvature Efy with load
91 PEY3 =  ParameterSet.PEY3   ; %Zero order camber dependency of
       curvature Efy
92 PEY4 =  ParameterSet.PEY4   ; %Variation of curvature Efy with camber
93 PEY5 =  ParameterSet.PEY5   ; %Variation of curvature Efy with camber
       squared
94 PKY1 =  ParameterSet.PKY1   ; %Maximum value of stiffness Kfy./Fznom
95 PKY2 =  ParameterSet.PKY2   ; %Load at which Kfy reaches maximum
       value
96 PKY3 =  ParameterSet.PKY3   ; %Variation of Kfy./Fznom with camber
97 PKY4 =  ParameterSet.PKY4   ; %Curvature of stiffness Kfy
98 PKY5 =  ParameterSet.PKY5   ; %Peak stiffness variation with camber
       squared
99 PKY6 =  ParameterSet.PKY6   ; %Fy camber stiffness factor
```

```
100 PKY7 =  ParameterSet.PKY7   ; %Vertical load dependency of camber
    stiffness
101 PHY1 =  ParameterSet.PHY1   ; %Horizontal shift Shy at Fznom
102 PHY2 =  ParameterSet.PHY2   ; %Variation of shift Shy with load
103 PVY1 =  ParameterSet.PVY1   ; %Vertical shift in Svy./Fz at Fznom
104 PVY2 =  ParameterSet.PVY2   ; %Variation of shift Svy./Fz with load
105 PVY3 =  ParameterSet.PVY3   ; %Variation of shift Svy./Fz with camber
106 PVY4 =  ParameterSet.PVY4   ; %Variation of shift Svy./Fz with camber
     and load
107 PPY1 =  ParameterSet.PPY1   ; %influence of inflation pressure on
    cornering stiffness
108 PPY2 =  ParameterSet.PPY2   ; %influence of inflation pressure on
    dependency of nominal tyre load on cornering stiffness
109 PPY3 =  ParameterSet.PPY3   ; %linear influence of inflation pressure
     on lateral peak friction
110 PPY4 =  ParameterSet.PPY4   ; %quadratic influence of inflation
    pressure on lateral peak friction
111 PPY5 =  ParameterSet.PPY5   ; %Influence of inflation pressure on
    camber stiffness
112 PTY1 =  ParameterSet.PTY1  ; %Influence of tread temperature on
    cornering stiffness
113 PTY2 =  ParameterSet.PTY2  ; %Influence of tread temperature on
    location of cornering stiffness peak
114 PTY3 =  ParameterSet.PTY3  ; %Linear temperature effect on peak
    lateral friction
115 PTY4 =  ParameterSet.PTY4  ; %Quadratic temperature effect on peak
    lateral friction
116 RBY1 =  ParameterSet.RBY1; %Slope factor for combined Fy reduction
117 RBY2 =  ParameterSet.RBY2; %Variation of slope Fy reduction with
    alpha
118 RBY3 =  ParameterSet.RBY3; %Shift term for alpha in slope Fy
    reduction
119 RBY4 =  ParameterSet.RBY4; %Influence of camber on stiffness of Fy
    combined
120 RCY1 =  ParameterSet.RCY1; %Shape factor for combined Fy reduction
121 REY1 =  ParameterSet.REY1; %Curvature factor of combined Fy
122 REY2 =  ParameterSet.REY2; %Curvature factor of combined Fy with load
123 RHY1 =  ParameterSet.RHY1; %Shift factor for combined Fy reduction
124 RHY2 =  ParameterSet.RHY2; %Shift factor for combined Fy reduction
    with load
125 RVY1 =  ParameterSet.RVY1; %Kappa induced side force Svyk./Muy.*Fz at
     Fznom
126 RVY2 =  ParameterSet.RVY2; %Variation of Svyk./Muy.*Fz with load
127 RVY3 =  ParameterSet.RVY3; %Variation of Svyk./Muy.*Fz with camber
128 RVY4 =  ParameterSet.RVY4; %Variation of Svyk./Muy.*Fz with alpha
129 RVY5 =  ParameterSet.RVY5; %Variation of Svyk./Muy.*Fz with kappa
130 RVY6 =  ParameterSet.RVY6; %Variation of Svyk./Muy.*Fz with atan(
    kappa)
131
```

```
% Preliminary calculations
% Some basic calculations are done before calculating forces and
    moments

% Velocities in point S (slip point)
Vsx = -kappa.*abs(Vcx); % [Eqn (4.E5) Page 181 - Book]
Vsy = tan(alpha).*abs(Vcx); % [Eqn (2.12) Page 67 - Book] and [(4.E3)
    Page 177 - Book]
% Important Note:
% Due to the ISO sign convention, equation 2.12 does not need a
% negative sign. The Pacejka book is written in adapted SAE.
Vs = sqrt(Vsx.^2+Vsy.^2); % [Eqn (3.39) Page 102 - Book] -> Slip
    velocity of the slip point S

% Velocities in point C (contact)
Vcy = Vsy; % Assumption from page 67 of the book, paragraph above Eqn
    (2.11)
Vc = sqrt(Vcx.^2+Vcy.^2); % Velocity of the wheel contact centre C,
    Not described in the book but is the same as [Eqn (3.39) Page 102
    - Book]

% Effect of having a tire with a different nominal load
Fz0_prime =  LFZO.*Fz0; % [Eqn (4.E1) Page 177 - Book]
%Fz0_prime = Fz0; % NON HO MESSO LFZO NEGLI INPUT

% Normalized change in vertical load
dfz = (Fz - Fz0_prime)./Fz0_prime; % [Eqn (4.E2a) Page 177 - Book]

% Normalized change in inflation pressure
dpi = (p - pi0)./pi0; % [Eqn (4.E2b) Page 177 - Book]

% Normalized change in tread temperature
dT = (T-T0)./T0;

alpha_star = tan(alpha).*sign(Vcx); % [Eqn (4.E3) Page 177 - Book]
gamma_star = sin(gamma); % [Eqn (4.E4) Page 177 - Book]

% Slippery surface with friction decaying with increasing (slip)
    speed
LMUX_star = LMUX./(1 + LMUV.*Vs./V0); % [Eqn (4.E7) Page 179 - Book]
LMUY_star = LMUY./(1 + LMUV.*Vs./V0); % [Eqn (4.E7) Page 179 - Book]

% Digressive friction factor
% On Page 179 of the book is suggested Amu = 10, but after
% comparing the use of the scaling factors against TNO, Amu = 1
% was giving perfect match
Amu = 1;
LMUX_prime = Amu.*LMUX_star./(1+(Amu-1).*LMUX_star); % [Eqn (4.E8)
    Page 179 - Book]
```

```
173 LMUY_prime = Amu.*LMUY_star./(1+(Amu-1).*LMUY_star); % [Eqn (4.E8)
    Page 179 - Book]
174
175 % Epsilon
176 % Parameters not specified in the TIR file
177 % Used to avoid low speed singularity
178 epsilon  = 1e-6; % [Eqn (4.E6a) Page 178 - Book]
179 epsilonv = epsilon;
180 epsilonx = epsilon;
181 epsilonk = epsilon;
182 epsilony = epsilon;
183 epsilonr = epsilon;
184
185 zeta0 = 1;
186 zeta1 = ones(size(Fz));
187 zeta2 = ones(size(Fz));
188 zeta3 = ones(size(Fz));
189 zeta4 = ones(size(Fz));
190
191 % Pure Longitudinal Fx0
192
193 Cx = PCX1.*LCX; % (> 0) (4.E11)
194 mux = (PDX1 + PDX2.*dfz).*(1 + PPX3.*dpi + PPX4.*dpi.^2).*(1 - PDX3.*
    gamma.^2).*LMUX_star; % (4.E13)
195 mux(Fz==0) = 0; % Zero Fz correction
196 DxBase = mux.*Fz.*zeta1; % (> 0) (4.E12)
197 Dx = (1 + PTX3.*dT + PTX4.*dT.^2).*DxBase;
198 KxkBase = Fz.*(PKX1 + PKX2.*dfz).*exp(PKX3.*dfz).*(1 + PPX1.*dpi +
    PPX2.*dpi.^2).*LKX;  % (= BxCxDx = dFxo./dkx at kappax = 0) (= Cfk
    ) (4.E15)
199 Kxk = (1 + PTX1.*dT + PTX2.*dT.^2).*KxkBase;
200
201 signDx = sign(Dx);
202 signDx(signDx == 0) = 1; % If [Dx = 0] then [sign(0) = 0]. This is
    done to avoid [Kxk / 0 = NaN] in Eqn 4.E16
203
204 Bx = Kxk./(Cx.*Dx + epsilonx.*signDx); % (4.E16) [sign(Dx) term
    explained on page 177]
205 SHx = (PHX1 + PHX2.*dfz).*LHX; % (4.E17)
206 SVx = Fz.*(PVX1 + PVX2.*dfz).*LVX.*LMUX_prime.*zeta1; % (4.E18)
207
208 kappax = kappa + SHx; % (4.E10)
209
210 Ex = (PEX1 + PEX2.*dfz + PEX3.*dfz.^2).*(1 - PEX4.*sign(kappax)).*LEX
    ; % (<=1) (4.E14)
211
212 % Pure longitudinal force
213 Fx0 = Dx.*sin(Cx.*atan(Bx.*kappax-Ex.*(Bx.*kappax-atan(Bx.*kappax))))
    +SVx; % (4.E9)
```

```
214
215 % Combined Fx
216
217 Cxa = RCX1; % (4.E55)
218 Exa = REX1 + REX2.*dfz; % (<= 1) (4.E56)
219
220 SHxa = RHX1; % (4.E57)
221 Bxa = (RBX1 + RBX3.*gamma_star.^2).*cos(atan(RBX2.*kappa)).*LXAL; %
    (> 0) (4.E54)
222
223 alphas = alpha_star + SHxa; % (4.E53)
224
225 Gxa0 = cos(Cxa.*atan(Bxa.*SHxa-Exa.*(Bxa.*SHxa-atan(Bxa.*SHxa)))); %
    (4.E52)
226 Gxa = cos(Cxa.*atan(Bxa.*alphas-Exa.*(Bxa.*alphas-atan(Bxa.*alphas)))
    )./Gxa0; % (> 0)(4.E51
227
228 Fx = Gxa.*Fx0; % (4.E50)
229
230 % Pure Lateral Fy0
231
232 Kya = (1 + PTY1.*dT).*PKY1.*Fz0_prime.*(1 + PPY1.*dpi).*(1 - PKY3.*
    abs(gamma_star)).*sin(PKY4.*atan((Fz./Fz0_prime)./((PKY2+PKY5.*
    gamma_star.^2).*(1+PPY2.*dpi).*(1+PTY2.*dT)))).*zeta3.*LKY; % (=
    ByCyDy = dFyo./dalphay at alphay = 0) (if gamma =0: =Kya0 = CFa) (
    PKY4=2)(4.E25)
233
234 SVyg = Fz.*(PVY3 + PVY4.*dfz).*gamma_star.* LKYC .* LMUY_prime .*
    zeta2; % (4.E28)
235
236 Kyg0 = Fz.*(PKY6 + PKY7 .*dfz).*(1 + PPY5.*dpi).*LKYC; % (=dFyo./
    dgamma at alpha = gamma = 0) (= CFgamma) (4.E30)
237 %Kya0 = PKY1.*Fz0_prime.*(1 + PPY1.*dpi).*(1 - PKY3.*abs(0)).*sin(
    PKY4.*atan((Fz./Fz0_prime)./((PKY2+PKY5.*0.^2).*(1+PPY2.*dpi)))).*
    zeta3.*LKY;
238
239 signKya = sign(Kya);
240 signKya(signKya == 0) = 1; % If [Kya = 0] then [sign(0) = 0]. This is
     done to avoid [num / 0 = NaN] in Eqn 4.E27
241
242 SHy = (PHY1 + PHY2.*dfz).* LHY + ((Kyg0 .*gamma_star - SVyg)./(Kya +
    epsilonk.*signKya)).*zeta0 +zeta4 -1; % (4.E27) [sign(Kya) term
    explained on page 177]
243
244 SVy = Fz.*(PVY1 + PVY2.*dfz).*LVY.*LMUY_prime.*zeta2 + SVyg; % (4.E29
    )
245 alphay = alpha_star + SHy; % (4.E20)
246 Cy = PCY1.*LCY; % (> 0) (4.E21)
```

```
247 muy = (PDY1 + PDY2 .* dfz).*(1 + PPY3.*dpi + PPY4 .*dpi.^2).*(1 -
        PDY3.*gamma_star.^2).*LMUY_star; % (4.E23)
248
249 DyBase = muy.*Fz.*zeta2; % (4.E22)
250 Dy = (1 + PTY3 .* dT + PTY4 .* dT.^2) .* DyBase;
251
252 signAlphaY = sign(alphay);
253 signAlphaY(signAlphaY == 0) = 1;
254 Ey = (PEY1 + PEY2.*dfz).*(1 + PEY5.*gamma_star.^2 - (PEY3 + PEY4.*
        gamma_star).*signAlphaY).*LEY; % (<=1)(4.E24)
255
256 signDy = sign(Dy);
257 signDy(signDy == 0) = 1; % If [Dy = 0] then [sign(0) = 0]. This is
        done to avoid [Kya / 0 = NaN] in Eqn 4.E26
258 By = Kya./(Cy.*Dy + epsilony.*signDy); % (4.E26) [sign(Dy) term
        explained on page 177]
259
260 % Pure lateral force
261 Fy0 = Dy .* sin(Cy.*atan(By.*alphay-Ey.*(By.*alphay - atan(By.*alphay
        ))))+ SVy; % (4.E19)
262
263 % Combined Fy
264
265 DVyk = muy.*Fz.*(RVY1 + RVY2.*dfz + RVY3.*gamma_star).*cos(atan(RVY4
        .*alpha_star)).*zeta2; % (4.E67)
266 SVyk = DVyk.*sin(RVY5.*atan(RVY6.*kappa)).*LVYKA; % (4.E66)
267 SHyk = RHY1 + RHY2.*dfz; % (4.E65)
268 Eyk = REY1 + REY2.*dfz; % (<=1) (4.E64)
269 Cyk = RCY1; % (4.E63)
270 Byk = (RBY1 + RBY4.*gamma_star.^2).*cos(atan(RBY2.*(alpha_star - RBY3
        ))).*LYKA; % (> 0) (4.E62)
271 kappas = kappa + SHyk; % (4.E61)
272
273 Gyk0 = cos(Cyk.*atan(Byk.*SHyk - Eyk.*(Byk.*SHyk - atan(Byk.*SHyk))))
        ; % (4.E60)
274 Gyk = cos(Cyk.*atan(Byk.*kappas - Eyk.*(Byk.*kappas-atan(Byk.*kappas)
        ))))./Gyk0; % (> 0)(4.E59)
275
276 Fy = Gyk.*Fy0 + SVyk; % (4.E58)
277
278
279 output(:,1) = Fx;
280 output(:,2) = Fy;
281
282 end
```

Bibliography

[1] J. Balkwill (2018). *Performance Vehicle Dynamics*, pp. 19-21.

[2] G. Genta & L. Morello (2009). *The Automotive Chassis - Volume 1*, pp. 90-95.

[3] *https://www.millikenresearch.com/fsaettc.html*, Calspan Corporation & FSAE TTC.

[4] A. Sorniotti (2009). *Tire Thermal Model for Enhanced Vehicle Dynamics Simulation.*

[5] A. J. Tremlett & J. N. Limebeer (2016). *Optimal tyre usage for a Formula One car*, Vehicle System Dynamics.

[6] D. P. Kelly a & R. S. Sharp (2012). *Time-optimal control of the race car: influence of a thermodynamic tyre model*, Vehicle System Dynamics.

[7] D. Giordano (2009). *Temperature prediction of high performance racing tyres, development and validation of a physical thermal model*, Università degli Studi di Napoli.

[8] W.J. West & D. J. N. Limebeer (2020). *Optimal tyre management for a high-performance race car*, Vehicle System Dynamics.

[9] A. Hackl, C. Scherndl, W. Hirschberg & C. Lex (2017). *Experimental Validation of Various Temperature Models for Semi-Physical Tyre Model Approaches*, IOP Conf. Ser.: Mater. Sci. Eng.

[10] P. Cattani, L. Cattani & A. Magrini (2023). *Tyre–Road Heat Transfer Coefficient Equation Proposal.*

[11] Hans B. Pacejka (2006). *Tyre and Vehicle Dynamics, 2nd Edition*, Delft University of Technology.

[12] D. Harsh & B. Shyrokau (2019). *Tire Model with Temperature Effects for Formula SAE Vehicle.*

[13] M. Furlan (2024). *MFeval (https://www.mathworks.com/matlabcentral/fileexchange/63618-mfeval)*, MATLAB Central File Exchange.

[14] I. J.M.Besselink, A. J.C. Schmeitz H.B. Pacejka (2010). *An improved Magic Formula/Swift tyre model that can handle inflation pressure changes)*, Vehicle System Dynamics.

List of Tables

List of Figures